Monte Carlo perturbation calculation for geometry change in fixed source problems with the perturbation source method

Toshihiro Yamamoto[a*], Hiroki Sakamoto[b]

[a]*Institute for Integrated Radiation and Nuclear Science, Kyoto University, 2 Asashiro Nishi, Kumatori-cho, Sennan-gun, Osaka, 590-0494, Japan*

[b]*Independent researcher, Radiation Dose Analysis and Evaluation Network, 4-13-14, Kokubunji-shi, Tokyo, 185-0001, Japan*

Abstract

The perturbation source method (PSM), which is a Monte Carlo perturbation calculation method, is applied to geometry changes in fixed-source neutron transport problems. In PSM, perturbation particles that represent the flux difference due to the changes in geometry are explicitly tracked within the perturbed system. A perturbation calculation for geometry change can be performed by replacing the material in a perturbed region with the material that occupies the adjoining region beyond the geometry change. The efficiency of the PSM can be enhanced by adding a pseudo-scattering cross section to the perturbed region. For geometry changes where the perturbed region is small, PSM exhibits excellent performance compared to the two independent runs before and after the perturbation if optimized pseudo-scattering cross sections are used. This method can also be applied to perturbation due to an external boundary change. Although the correlated sampling method (CS) is another available Monte Carlo method for geometry change, PSM largely outperforms CS in terms of computational efficiency for the numerical examples tested in this study.

Keywords: Monte Carlo; perturbation; fixed source; neutron

1. Introduction

Accurate estimation of flux difference due to a small perturbation (cross section, geometry) is one of the weaknesses of the Monte Carlo radiation transport calculations. Thus far, several Monte Carlo perturbation techniques have been developed to overcome this weakness, such as the

* Corresponding author. E-mail address: toshihiro.yamamoto223@gmail.com (T. Yamamoto)

correlated sampling method (CS) (Spanier and Gelbard, 1969; Bernnat, 1974; Nakagawa and Asaoka, 1978; He and Su, 2010, 2011; Kiedrowski, 2017) and the differential operator sampling method (DOS) (Rief, 1984; McKinney and Iverson, 1996; Densmore et al., 1997; Nagaya and Mori, 2005; Favorite, 2009; Raskach, 2009; Nagaya, 2012; Jinaphanh et al., 2016; Kiedrowski, 2017; Yamamoto and Sakamoto, 2019a, 2019b, 2020). The characteristics of these widely used perturbation methods have long been investigated, and the advantages and weaknesses of the methods have been evaluated. The weakness of CS is that it involves an unbounded statistical uncertainty for a large perturbation (Rief, 1984). Meanwhile, DOS is a method that yields the derivative of the flux with respect to a cross section instead of yielding the flux difference. Thus, DOS provides an approximate flux difference by the Taylor series expansion with respect to a cross section. The higher-order derivatives are considered, and more accurate results can be obtained. Thus, while the flux difference can be estimated by lower order derivatives for a small cross section perturbation, accurate estimation for a large perturbation requires a large number of higher-order derivatives.

This paper focuses on fixed-source Monte Carlo perturbation calculations for change in geometry. Perturbation calculations for geometry change are powerful methods for identifying the effect of uncertainties in material size or location. Perturbation due to geometry change can be represented by replacing a material in a perturbed region with the material that occupies the adjoining region beyond the geometry change. The change in geometry of an external boundary where a vacuum boundary condition is imposed is equivalent to the exchange between the vacuum and the outermost material. The cross-section perturbation due to geometry change in most cases may presumably exceed the range of "small perturbation" for which DOS and CS can provide accurate results even if the geometry change itself is small. Therefore, the well-known Monte Carlo perturbation methods, DOS and CS, may not be suitable for calculating the geometry change.

Another robust and exact method for Monte Carlo fixed source perturbation calculations, which is dubbed as "the perturbation source method" (PSM), was formerly proposed by Matthes,

(1972), Preeg and Tsang (1982), and Lux and Koblinger (1991). Although PSM had drawn little interest for decades as a Monte Carlo perturbation method, it was revisited by Sakamoto and Yamamoto (2017) and improved to increase the computational efficiency. Recently, the fundamental theory of PSM was extended to sensitivity analyses in fixed source calculations (Yamamoto and Sakamoto, in press). PSM is expected to be a Monte Carlo perturbation calculation method that may be applied to geometry change owing to its robustness and efficiency.

In Section 2, the fundamentals of PSM are revisited, and its application to geometry change is presented. In Section 3, some numerical examples of PSM are presented, and its superiority over other perturbation methods such as CS is exemplified. A summary and conclusions are provided in Section 4.

2. Theory of perturbation source method

2.1 Transport equation for flux difference due to perturbation

The theory of the perturbation source method (PSM) is briefly reviewed, although it has already been presented in previous publications (e.g., Sakamoto and Yamamoto, 2017). The fixed-source radiation transport equation in a non-multiplying system is given by:

$$\boldsymbol{H}\phi(\boldsymbol{r},\boldsymbol{\Omega},E) = S(\boldsymbol{r},\boldsymbol{\Omega},E), \tag{1}$$

where

$$\boldsymbol{H}\phi(\boldsymbol{r},\boldsymbol{\Omega},E) \equiv \boldsymbol{\Omega}\cdot\boldsymbol{\nabla}\phi(\boldsymbol{r},\boldsymbol{\Omega},E) + \Sigma_t(\boldsymbol{r},E)\phi(\boldsymbol{r},\boldsymbol{\Omega},E) - \int_{4\pi} d\boldsymbol{\Omega}' \int dE' \Sigma_s(\boldsymbol{r},\boldsymbol{\Omega}'\to\boldsymbol{\Omega},E'\to E)\phi(\boldsymbol{r},\boldsymbol{\Omega}',E'), \tag{2}$$

$\phi(\boldsymbol{r},\boldsymbol{\Omega},E) =$ the flux at position $\boldsymbol{r}$ with energy E and direction $\boldsymbol{\Omega}$, $S(\boldsymbol{r},\boldsymbol{\Omega},E) =$ external source term, $\Sigma_t =$ total cross section, and $\Sigma_s =$ scattering cross section. When the cross sections, Σ_t and Σ_s, change to $\Sigma_t + \Delta\Sigma_t$ and $\Sigma_s + \Delta\Sigma_s$, respectively, Eq. (1) changes to

$$(\boldsymbol{H} + \Delta\boldsymbol{H})\big(\phi(\boldsymbol{r},\boldsymbol{\Omega},E) + \delta\phi(\boldsymbol{r},\boldsymbol{\Omega},E)\big) = S(\boldsymbol{r},\boldsymbol{\Omega},E), \tag{3}$$

where

$$\Delta\boldsymbol{H}(\cdots) \equiv \Delta\Sigma_t(\boldsymbol{r},E)(\cdots) - \int_{4\pi} d\boldsymbol{\Omega}' \int dE' \Delta\Sigma_s(\boldsymbol{r},\boldsymbol{\Omega}'\to\boldsymbol{\Omega},E'\to E)(\cdots)\,, \tag{4}$$

where $\delta\phi$ is the flux change due to the changes in cross section. It is assumed that the external

source term S is kept constant before and after the perturbation. Subtracting Eq. (1) from Eq. (3) yields the transport equation for $\delta\phi$

$$(\boldsymbol{H} + \Delta\boldsymbol{H})\delta\phi(\boldsymbol{r}, \boldsymbol{\Omega}, E) = -\Delta\boldsymbol{H}\phi(\boldsymbol{r}, \boldsymbol{\Omega}, E). \quad (5)$$

The right-hand side of Eq. (5) can be rewritten as

$$-\Delta\boldsymbol{H}\phi(\boldsymbol{r}, \boldsymbol{\Omega}, E) = -\Delta\Sigma_t(\boldsymbol{r}, E)\phi(\boldsymbol{r}, \boldsymbol{\Omega}, E)$$

$$+\int_{4\pi} d\boldsymbol{\Omega}' \int dE' \Delta\Sigma_s(\boldsymbol{r}, \boldsymbol{\Omega}' \to \boldsymbol{\Omega}, E' \to E)\phi(\boldsymbol{r}, \boldsymbol{\Omega}', E'). \quad (6)$$

The right-hand side of Eq. (5) is the source term for the transport equation of $\delta\phi$. The flux, ϕ, on the right-hand side is the flux in the unperturbed system. Eq. (5) does not involve any approximation, and the flux change, $\delta\phi$, can be obtained by solving Eq. (5).

2.2 Monte Carlo algorithm of PSM

In a Monte Carlo algorithm proposed by Sakamoto and Yamamoto (2017), the random walk process for solving Eq. (5) is performed for solving Eq. (1) for the fixed-source problem in the unperturbed system. The entire process is composed of two modes: the fixed source mode and the perturbation mode. The Monte Carlo algorithm for solving Eq. (5) is as follows:

(1) The calculation starts with the fixed-source mode for solving Eq. (1). At the beginning of the fixed source mode, a source particle is emitted from the external source according to the source term S, and the particle is tracked in the *unperturbed* system.

(2) When the particle undergoes collision in a perturbed region, the random walk process in the fixed source mode is suspended. Then, the calculation mode is switched to the perturbation mode.

(3) As shown in Eq. (6), the source term for the flux difference is composed of two terms. The first is caused by the change in the total cross section. A source particle representing the change in total cross-section (the first term on the right-hand side of Eq. (6)) is emitted from the collision point. The weight of the source particle is given by:

$$W_{\mathrm{t}} = -(\Sigma_t^p - \Sigma_t^{up})\frac{W}{\Sigma_t^{un}}, \quad (7)$$

where W is the weight of the colliding particle in the fixed source mode, and Σ_t^p and Σ_t^{un} are the perturbed and unperturbed total cross sections, respectively. The energy and direction of the source particle are the same as those of the colliding particle. The particle, which is called "perturbation particle" hereafter, is tracked in the *perturbed* system until its death.

(4) The second source term is caused by the change in the scattering cross section, which is represented by the second term on the right-hand side of Eq. (6). The change in the scattering cross section is divided into two components: the change in the total scattering cross section and the change in the collision law. The direction $\boldsymbol{\Omega}'$ and energy E' of the source particle were sampled from the collision law in the *unperturbed* system. The weight of the source particle for the change in the total scattering cross section is given by

$$W_{\mathrm{s}} = (\Sigma_s^p - \Sigma_s^{un}) \frac{W}{\Sigma_t^{un}}, \tag{8}$$

where Σ_s^p and Σ_s^{un} are the perturbed and unperturbed total scattering cross-sections, respectively. The weight of the source particle corresponding to the change in the collision law is given by

$$W_{\mathrm{a}} = \frac{f^p(\boldsymbol{\Omega}\cdot\boldsymbol{\Omega}', E \to E') - f^{un}(\boldsymbol{\Omega}\cdot\boldsymbol{\Omega}', E \to E')}{f^{un}(\boldsymbol{\Omega}\cdot\boldsymbol{\Omega}', E \to E')} \Sigma_s^p \frac{W}{\Sigma_t^{un}}, \tag{9}$$

where $f(\boldsymbol{\Omega}\cdot\boldsymbol{\Omega}', E \to E')$ is the probability that the direction and energy after scattering becomes $\boldsymbol{\Omega}'$ and E' from $\boldsymbol{\Omega}$ and E, respectively. The superscript *p* or *un* on *f* denotes that the scattering law belongs to the perturbed or unperturbed system, respectively. In addition to the source particle defined in Eq. (7), another source particle with a weight of $W_{\mathrm{s}} + W_a$ is emitted from the collision point. This perturbation particle is also tracked in the *perturbed* system until its death. Eq. (9) is available on the condition that the ranges of $\boldsymbol{\Omega}\cdot\boldsymbol{\Omega}'$ and E' in the unperturbed system include their entire range in the perturbed system. Thus, voids cannot represent a material in an unperturbed system because $\boldsymbol{\Omega}\cdot\boldsymbol{\Omega}'$ is always unity in a void. In addition, a material containing light hydrogen, such as light water, is not available for an unperturbed system because the term $\boldsymbol{\Omega}\cdot\boldsymbol{\Omega}'$ for light hydrogen is not below zero, whereas $\boldsymbol{\Omega}\cdot\boldsymbol{\Omega}'$ of a material that does not contain

light hydrogen ranges between −1 and 1.

(5) After steps (3) and (4) are completed, the calculation mode is returned to the fixed source mode. Then, the fixed source calculation that is suspended in step (2) is resumed.

(6) After the particle that is emitted in step (1) is killed, return to step (1) and another new source particle is emitted.

(7) Steps (1) through (6) are repeated until the desired statistics are obtained.

A flowchart of the PSM is shown in Fig. 1 in (Sakamoto and Yamamoto, 2017). The flux calculated in steps (3) and (4) represents the change in flux $\delta\phi$ due to the perturbation.

2.3 Improvement of PSM efficiency

The efficiency of PSM can be improved by increasing the number of perturbation particles that are emitted in steps (3) and (4), especially when the perturbed region is small and fewer collisions occur in the region. Because the number of perturbation particles is proportional to the number of collisions in the perturbed region, the efficiency can be enhanced by increasing the number of collisions. For this purpose, a pseudo-scattering cross section was added to the perturbed region. The total cross section in the perturbed region is multiplied by a factor of C (>1):

$$\Sigma_t^* = C\Sigma_t, \tag{10}$$

where Σ_t^* is a pseudo-total cross section. The fixed source mode calculation uses Σ_t^* for the total cross section in the perturbed region. The number of perturbation particles that was increased forcibly is compensated for by decreasing the weight of the perturbation particles as follows:

$$W_{\mathrm{t}}^* = \frac{1}{C} W_t, \tag{11}$$

$$W_{\mathrm{s}}^* + W_a^* = \frac{1}{C}(W_s + W_a)\,. \tag{12}$$

After steps (3) and (4) in Section 2.2, a pseudo random number ξ between 0 and 1 is generated. If $\xi < 1/\mathrm{C}$, the collision is accepted as a real collision. Otherwise, the collision is rejected and the particle continues flying without any change in the weight, energy, and direction.

2.4 PSM for geometry change

(1) Displacement of the internal material

In this section, we discuss how PSM treats the geometry change in a fixed source calculation. Fig. 1 shows an example where material 2 is displaced upward within material 1. This change in geometry can be attained by replacing material 1 with material 2 in region 1, and replacing material 2 with material 1 in region 2. For example, when a particle undergoes a collision in region 1 in the fixed source mode calculation, Σ_t^p and Σ_t^{un} in Eq. (7) are the total cross sections of material 2 and material 1, respectively. Similarly, when a particle undergoes a collision in region 2, Σ_t^p and Σ_t^{un} are the total cross sections of material 1 and material 2, respectively.

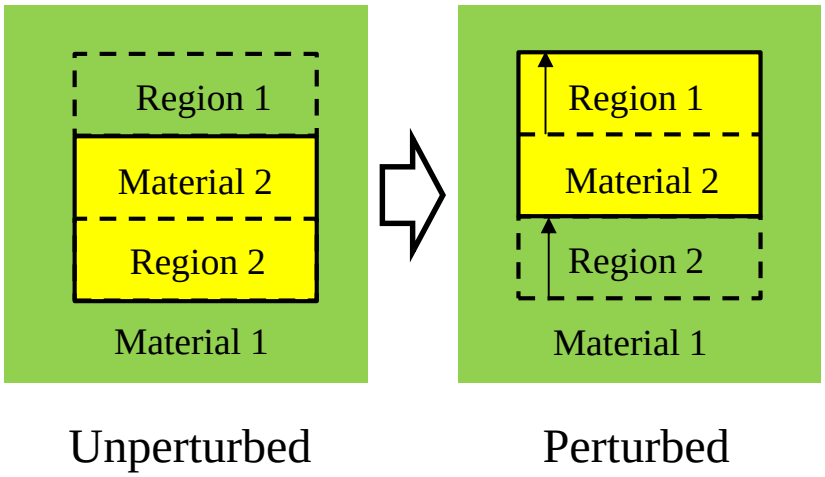

Fig. 1 Upward displacement of the material 2 within material 1.

[Fig. 1]

(2) External boundary changes

The geometry change of an external boundary exposed to vacuum is illustrated in Fig 2, where the upper external boundary recedes downward. This change in geometry is represented by replacing the material in region 1 with a void. If a non-void material is replaced with a void due to the change in geometry, PSM can be performed by setting

$$\Sigma_t^p = \Sigma_s^p = f^p(\boldsymbol{\Omega} \cdot \boldsymbol{\Omega}', E \to E') = 0, \tag{13}$$

in Eqs. (7), (8), and (9). For the reason stated in Section 2.2, voids cannot be replaced with a non-void material. Therefore, the change in geometry cannot be done in such a way that the void outside the external boundary is replaced with the material inside the boundary. In other words, the geometry change of an external boundary must be performed in the direction shown in Fig. 2 (from

(a) to (b)).

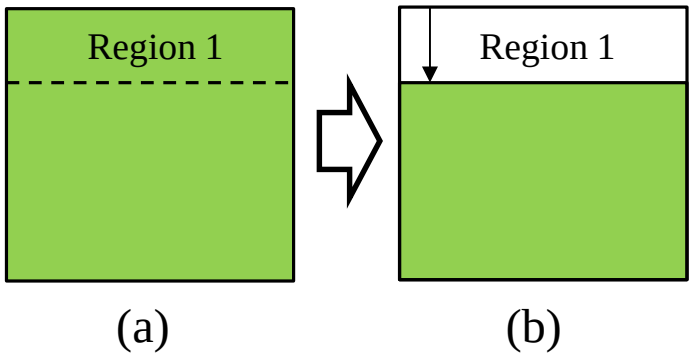

Fig. 2 Replacement of the material in the region 1 with void.

[Fig. 2]

(3) Displacement of internal voids or light water

PSM cannot directly treat the displacement of internal material illustrated in Fig. 1 when the internal material is void or light water, as already stated in Section 2.2. In such a case, the geometry change can be handled by performing two PSM calculations. First, an unperturbed system is set up by replacing material 2 in region 2 with material 1, as shown in the left part of Fig. 3. The first PSM calculation is performed for a perturbation where material 1 in region 1 is replaced with material 2, as shown in the upper right part of Fig. 3. The second PSM calculation is performed for a perturbation where material 1 in region 2 is replaced with material 2, as shown in the lower right part of Fig. 3. Let $\delta\phi_1$ and $\delta\phi_2$ be flux differences calculated in the first and second PSM calculations, respectively. Then, the flux difference $\delta\phi$ due to the upward displacement of the void or light water is eventually given by

$$\delta\phi = \delta\phi_1 - \delta\phi_2. \tag{14}$$

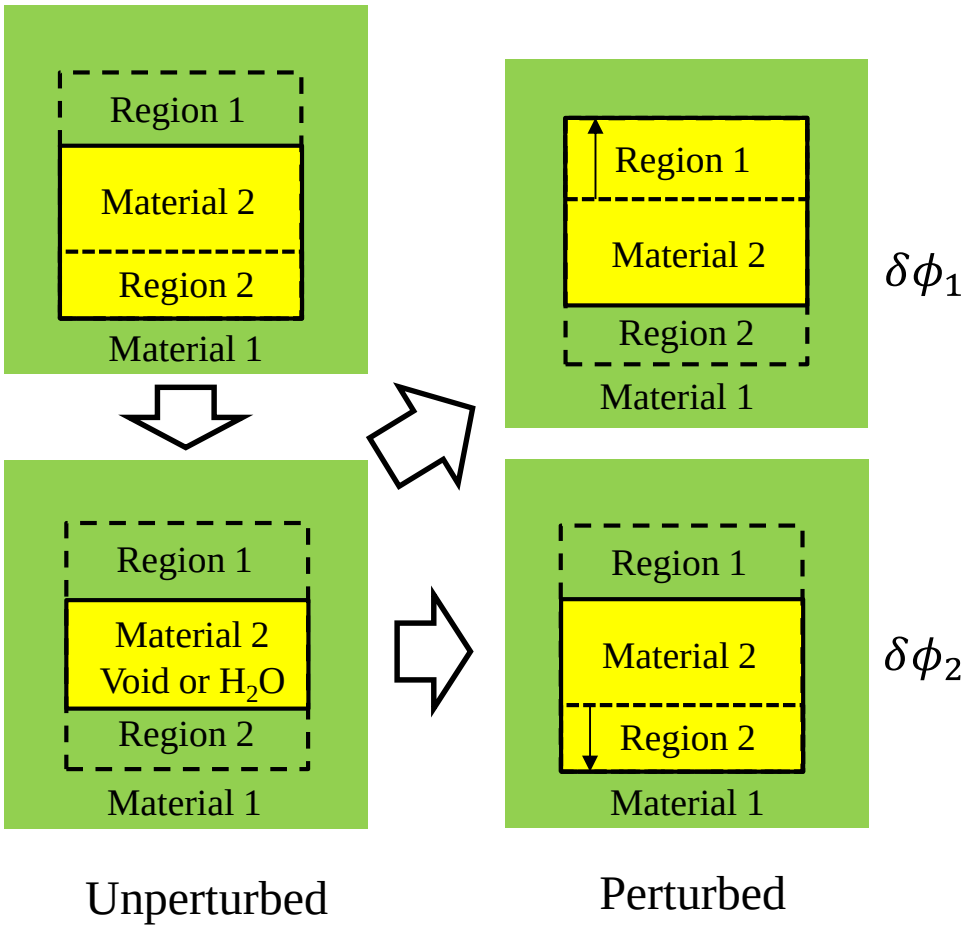

Fig. 3 Displacement of the material 2 made of void or light water.

[Fig. 3]

3. Numerical tests for geometry changes

3.1 Verification of PSM

Before presenting the results of PSM calculations for geometry change, the verification of PSM is presented for cross section change. All calculations in this study were performed for two-dimensional rectangular geometry. A line neutron beam entered perpendicular to the center of side 4 as shown in Fig. 4. Throughout this paper, the calculations were performed using the three-energy group constants, as shown in Tables 1, 2, and 3. Anisotropic scattering was considered up to the P_1 order. The upper and lower energy boundaries of the 2nd-energy group were 6.7 keV and 0.993 eV, respectively. The energy spectrum of the incident beam was $\phi_1 : \phi_2 : \phi_3 = 0.343 : 0.252 : 0.405$, which is a neutron spectrum in a light water reactor. The verification calculations were performed for rectangular graphite with a cross section of 2 × 2 cm, as shown in Fig. 4. This

unrealistically tiny geometry was chosen to ensure negligibly small statistical uncertainties in the reference solution, which is to be compared with the proposed method. The unperturbed system was composed of pure graphite. The perturbation was made by replacing a 0.6 × 0.7 cm rectangular region with light water. The dimensions shown in Fig. 4 were

a = 2 cm, b = 0.9 cm, c = 1.1 cm, d = 0.7 cm, and e = 0.6 cm.

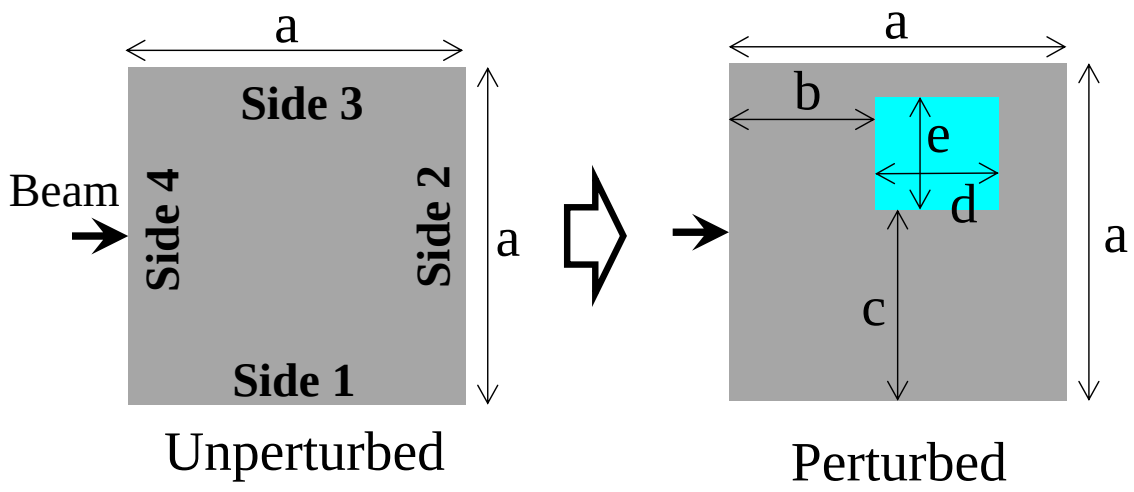

a = 2 cm, b = 0.9 cm, c = 1.1 cm, d = 0.7 cm, e = 0.6 cm.

Fig. 4 Geometry for verification of PSM (not to scale).

[Fig. 4]

The surface fluxes in the 3rd-energy group were calculated for the four external boundaries. Each time a particle escaped one of the four sides, the estimate of the surface flux on each side, $W/(\boldsymbol{n}\cdot\boldsymbol{\Omega})$, was calculated, where $W =$ weight of the particle, $\boldsymbol{\Omega} =$ direction vector of the particle, and $\boldsymbol{n}$ = the unit outward vector normal to the external boundary. The surface flux on side j (=1, 2, 3, and 4) is estimated as follows:

$$S_j = \frac{1}{M}\sum_i \frac{W_i}{\boldsymbol{n}_j \cdot \boldsymbol{\Omega}_i}, \tag{15}$$

where $W_i =$ the ith particle's weight escaping side j, i is summed over all particles escaping side j, and M is the total number of source neutrons. In the calculation of the PSM, W_i is the weight of the perturbation particle and S_j stands for the flux difference due to perturbation. The reference solution was obtained by the difference of the surface fluxes between two independent calculations

before and after perturbation, which is dubbed as the "direct" method hereafter.

For the comparison of PSM with another conventional Monte Carlo perturbation method, the correlated sampling method (CS) was applied to the problems in this study. In CS, particles of the perturbed history are forced to follow the same trajectories as the unperturbed history in phase space. The weight of the perturbed history in the CS was estimated at each collision in the perturbed region as

$$W_p' = W_p \cdot exp\left(-\left(\Sigma_t^p - \Sigma_t^{up}\right)s\right)\frac{\Sigma_s^{un}}{\Sigma_t^{un}} \cdot \frac{f^p(\boldsymbol{\Omega}\cdot\boldsymbol{\Omega}', E \to E')}{f^{un}(\boldsymbol{\Omega}\cdot\boldsymbol{\Omega}', E \to E')}, \quad (16)$$

where $W_p =$ the weight of the perturbed history before collision and *s* is the track length in the perturbed region. The surface flux difference by CS was estimated in the same manner as in Eq. (15):

$$\delta S_j = \frac{1}{M}\sum_i \frac{(W_{p,i} - W_{un,i})}{\boldsymbol{n}_j \cdot \boldsymbol{\Omega}_i}, \quad (17)$$

where $W_{p,i}$ and $W_{un,i}$ are the *i*th particle weight of the perturbed and unperturbed histories, respectively. The flux differences on sides 1, 2, and 3 calculated with PSM and CS are compared with the reference solution in Table 4. The CPU times required for the calculations on a single 3.40 GHz CPU are also shown in Table 4. Throughout this paper, all statistical uncertainties are one standard deviation, which are shown in parentheses in each table. The results of the PSM in Table 4 were obtained using the factor defined by Eq. (10), C =1. Table 4 shows that the flux differences calculated with the PSM agree precisely with the references. The results of the CS agree with the references within the statistical uncertainties. However, the agreement of CS with the references is not satisfactory, which is caused by the large statistical uncertainties in CS. Table 5 compares the relative figure-of-merit (FOM) defined by

$$FOM = \frac{1}{\sigma^2 T}, \quad (18)$$

where σ = one standard deviation of absolute uncertainty and *T* is the computation time. In terms of FOM, PSM is less effective than the direct method (two independent runs) even if the factor *C*

is increased up to 100. The perturbed region of this problem occupies approximately 10% of the entire domain, which is considered relatively large for a perturbed region. Thus, many perturbation particles were emitted from the perturbed region. CS is much less effective than PSM. It can thus be concluded that PSM can yield accurate results for flux differences, though it is not always an efficient method depending on the occupancy rate of a perturbed region.

[Tables 1, 2, 3, 4, 5]

3.2 Displacement of internal water in graphite

PSM was applied to a 20 × 20 cm rectangular graphite that includes a 1 × 2 cm internal light water region, as shown in Fig. 5. A change in geometry was induced by displacing the internal light water upward by 0.05 cm. The dimensions in Fig 5 were

a = 20 cm, b = 9 cm, c = 1 cm, d = 2 cm, and e = 0.05 cm.

Because this problem includes light water, PSM calculations were performed in two steps, as shown in Fig. 3. In CS, light water or voids cannot be replaced with another material in the same manner as in PSM, while material replacement in the inverse direction is possible. Thus, CS calculations were also performed using the same procedure as for PSM. The flux differences on the two surfaces, sides 1 and 3, and the relative FOMs are shown in Tables 6 and 7, respectively. The results for side 2 are omitted because the flux difference on side 2 was negligibly small. Table 6 shows that the direct method and CS can no longer yield statistically significant results for this small displacement. The computational efficiency of PSM without pseudo scattering (i.e., $C = 1$) is equivalent to the direct method. On the other hand, the fractional standard deviation of PSM with $C = 500$ is less than 3%, suggesting that PSM with the pseudo scattering method is an exclusively available calculation method for this small perturbation. As shown in Table 7, the computational efficiency of the PSM is improved with an increase in the factor C within the range of this numerical test.

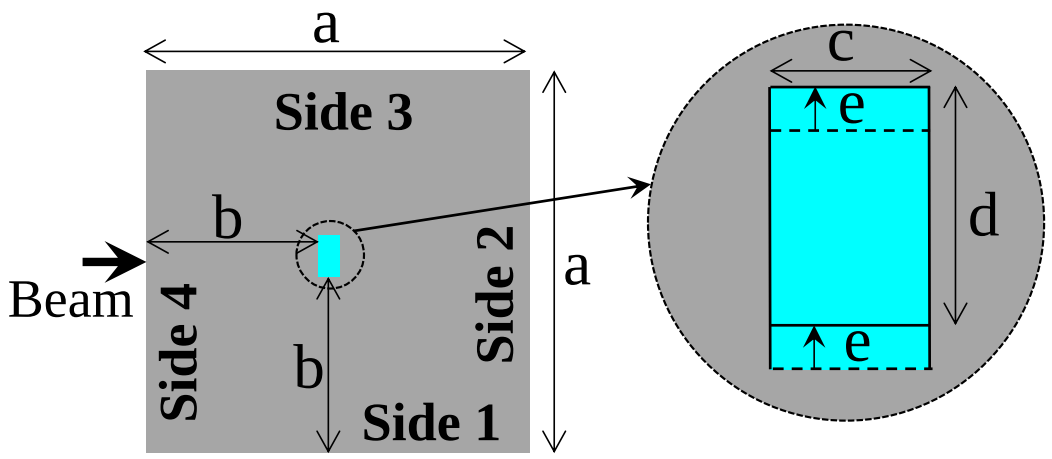

a = 20 cm, b = 9 cm, c = 1 cm , d = 2 cm, e = 0.05 cm.

Fig. 5 Geometry of slight displacement of internal material (light water or iron) (not to scale).

[Fig. 5] [Tables 6 and 7]

3.3 Displacement of internal iron in graphite

This section deals with the same geometry change as in Section 3.2, but the internal material is iron. Unlike in the previous section, two-step calculations are not necessary. The PSM and CS calculations can be performed only once according to the procedure shown in Fig. 1. The flux differences calculated with the direct method, PSM, and CS are shown in Table 8. The relative FOMs are listed in Table 9. The statistical uncertainties of the direct method and CS are much smaller in this problem compared with the previous problem. The FOMs of the PSM are larger than those of the direct method by a factor of thousands. The superiority of PSM to the direct method is more evident in this problem. Although the FOM of CS is smaller than that of PSM by a factor of tens, CS is also an available perturbation method for this problem.

[Tables 8, 9]

3.4 Verification of PSM for external boundary change

A verification calculation of the PSM for an external boundary change was performed again for a 2 × 2 cm graphite. In the perturbed system, a relatively large rectangular region near the beam source was removed from side 4, as shown in Fig. 6. The dimensions of the calculation shown in Fig. 6 were:

a = 2 cm, b = 0.7 cm, c = 0.5 cm, and d = 0.2 cm.

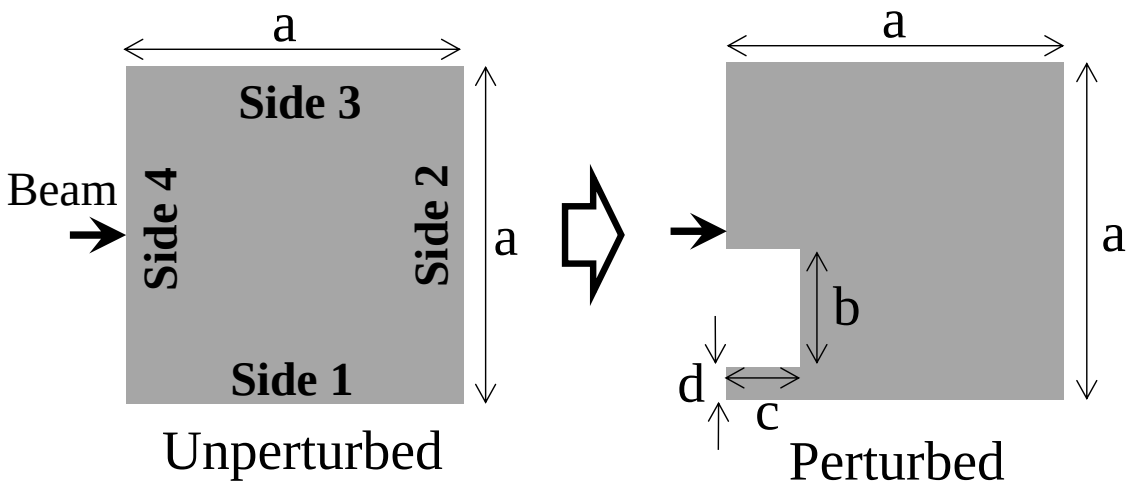

a = 2 cm, b = 0.7 cm, c = 0.5 cm, d= 0.2 cm

Fig. 6 Large change in external boundary (not to scale).

[Fig. 6]

The flux differences on sides 1, 2, and 3 calculated with PSM (C = 1) and CS are compared with the reference solution in Table 10. The flux differences calculated with the three methods agree precisely with each other. The two Monte Carlo perturbation methods, PSM and CS, can yield accurate results for the change in external boundary.

[Table 10]

3.5 Small external boundary change

PSM and CS were applied to an external boundary change in a 20 × 20 cm graphite from which a 0.5 × 0.5 cm rectangular region was removed from side 4, as shown in Fig. 7. The dimensions of the calculation are shown in Fig. 7. The flux differences on sides 1, 2, and 3 calculated with the direct method, PSM, and CS are shown in Table 11. The results calculated with the three methods agree with each other within the statistical uncertainties. The relative FOMs of the three methods are compared in Table 12. The FOMs of the PSM and CS are both much higher than that of the direct method. While CS is a Monte Carlo perturbation method that is applicable to an external boundary change, PSM outperforms CS by a factor of tens or hundreds for this problem.

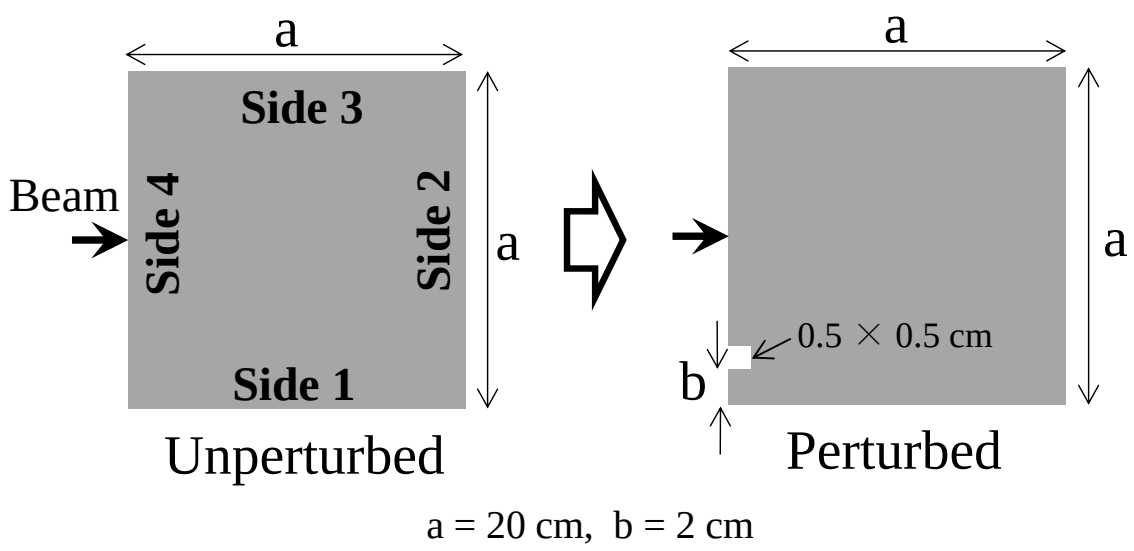

Fig. 7 Small change of external boundary (not to scale).

[Fig. 7] [Tables 11 and 12]

4. Conclusions

From the numerical tests, it can be concluded that the perturbation source method (PSM) and the correlated sampling method (CS) are Monte Carlo perturbation methods that are available for handling geometry changes in fixed source calculations. PSM is not always suitable for a large geometry change because too many perturbation sources must be emitted from the perturbed region. When the geometry change is large, PSM is less effective than the two independent runs before and after perturbation. On the other hand, PSM is the most effective Monte Carlo method for small geometry changes. The efficiency of the PSM is optimized by adjusting a pseudo-scattering cross section in the perturbed region. PSM, in particular, is an exclusively available method for a small displacement of internal light water within the surrounding material. PSM and CS can both perform perturbation calculations for the displacement of internal water or a void using a two-step procedure. Perturbation calculations for external boundary changes can be performed by replacing the material facing the external boundary with a void. PSM and CS are both applicable to external boundary changes. Regardless of the type of geometry change, PSM always outperforms CS in terms of computational efficiency within the range of the numerical tests performed in this study.

References

Bernnat, W., 1974. A Monte Carlo technique for local perturbations in multiplying systems, Proc. NEACRP Specialist Mtg., ANL-75-2, 261 (1974).

Densmore, J. D., McKinney, G.W., Hendricks, J.S., 1997. Correction to the MCNP perturbation feature for cross-section dependent tallies, LA-13374.

Favorite, J.A., 2009. On the accuracy of the differential operator Monte Carlo perturbation method for eigenvalue problems. Trans. Am. Nucl. Soc. 101, 460–462.

He, T., Su, B., 2010. On using correlated sampling to simulate small changes in system response by MCNP, Ann. Nucl. Energy 37, 34–42.

He, T., Su, B., 2011. Comparison between correlated sampling and the perturbation technique of MCNP5 for fixed-source problems, Ann. Nucl. Energy 38, 1318–1326.

Jinaphanh, A., Leclaire, N., Cochet, B., 2016. Continuous-energy sensitivity coefficients in the MORET code, Nucl. Sci. Eng. 184, 53–68.

Kiedrowski, B.C., 2017. Review of early 21st-century Monte Carlo perturbation and sensitivity techniques for *k*-eigenvalue radiation transport calculations. Nucl. Sci. Eng. 185, 426–444.

Lux, I., Koblinger, L., 1991. Monte Carlo Particle Transport Methods: Neutron and Photon Calculations, CRC Press.

McKinney, G.W., Iverson, J.L., 1996. Verification of the Monte Carlo differential operator technique for MCNP, Los Alamos National Laboratory, LA-13098.

Matthes, W., 1972. Calculation of reactivity perturbations with the Monte Carlo method, Nucl. Sci. Eng. 47, 234–237.

Nagaya, Y., Mori, T., 2005. Impact of perturbed fission source on the effective multiplication factor in Monte Carlo perturbation calculations, J. Nucl. Sci. Technol., 42, 428–441.

Nagaya, Y., 2012. Doctoral dissertation, Kyoto University (in Japanese) (The title translated from Japanese is “Study on reactor core analyses by the stochastic method”).

Nakagawa, M., Asaoka T., 1978. Improvement of correlated sampling Monte Carlo Methods for

reactivity calculations, J. Nucl. Sci. Technol. 15, 400–410.

Preeg, W.E., Tsang, J.S.K., 1982. Comparison of correlated Monte Carlo techniques, Trans. Am. Nucl. Soc. 43, 628–629.

Raskach, K. F., 2009. An improvement of the Monte Carlo generalized differential operator method by taking into account first- and second-order perturbations of fission source, Nucl. Sci. Eng. 162, 158–166.

Rief, H., 1984. Generalized Monte Carlo perturbation algorithms for correlated sampling and a second-order Taylor series approach. Ann. Nucl. Energy 9, 455–476.

Sakamoto, H., Yamamoto, T., 2017. Improvement and performance evaluation of the perturbation source method for an exact Monte Carlo perturbation calculation in fixed source problems, J. Compt. Phys. 345, 245–259.

Spanier, J., Gelbard, E.M., 1969. Monte Carlo principles and neutron transport problems, Addison-Wesley Publishing Company.

Yamamoto, T., Sakamoto, H., 2019a. A Monte Carlo technique for sensitivity analysis of alpha-eigenvalue with the differential operator sampling method. Ann. Nucl. Energy 127, 178–187.

Yamamoto, T., Sakamoto, H., 2019b. Two-step Monte Carlo sensitivity analysis of alpha- and gamma-eigenvalues with the differential operator sampling method. Ann. Nucl. Energy 133, 100–109.

Yamamoto, T., Sakamoto, H., 2020. Monte Carlo sensitivity analysis method for the effective delayed neutron fraction with the differential operator sampling method. Ann. Nucl. Energy 140, 107108.

Yamamoto, T., Sakamoto, H., (in press).

List of figures

Fig. 1 Upward displacement of material 2 within material 1.

Fig. 2 Replacement of the material in region 1 with void.

Monte Carlo perturbation calculation for geometry change in fixed source problems with the perturbation source method

Toshihiro Yamamoto[a*], Hiroki Sakamoto[b]

[a]*Institute for Integrated Radiation and Nuclear Science, Kyoto University, 2 Asashiro Nishi, Kumatori-cho, Sennan-gun, Osaka, 590-0494, Japan*

[b]*Independent researcher, Radiation Dose Analysis and Evaluation Network, 4-13-14, Kokubunji-shi, Tokyo, 185-0001, Japan*

Abstract

The perturbation source method (PSM), which is a Monte Carlo perturbation calculation method, is applied to geometry changes in fixed-source neutron transport problems. In PSM, perturbation particles that represent the flux difference due to the changes in geometry are explicitly tracked within the perturbed system. A perturbation calculation for geometry change can be performed by replacing the material in a perturbed region with the material that occupies the adjoining region beyond the geometry change. The efficiency of the PSM can be enhanced by adding a pseudo-scattering cross section to the perturbed region. For geometry changes where the perturbed region is small, PSM exhibits excellent performance compared to the two independent runs before and after the perturbation if optimized pseudo-scattering cross sections are used. This method can also be applied to perturbation due to an external boundary change. Although the correlated sampling method (CS) is another available Monte Carlo method for geometry change, PSM largely outperforms CS in terms of computational efficiency for the numerical examples tested in this study.

Keywords: Monte Carlo; perturbation; fixed source; neutron

1. Introduction

Accurate estimation of flux difference due to a small perturbation (cross section, geometry) is one of the weaknesses of the Monte Carlo radiation transport calculations. Thus far, several Monte Carlo perturbation techniques have been developed to overcome this weakness, such as the

* Corresponding author. E-mail address: toshihiro.yamamoto223@gmail.com (T. Yamamoto)

correlated sampling method (CS) (Spanier and Gelbard, 1969; Bernnat, 1974; Nakagawa and Asaoka, 1978; He and Su, 2010, 2011; Kiedrowski, 2017) and the differential operator sampling method (DOS) (Rief, 1984; McKinney and Iverson, 1996; Densmore et al., 1997; Nagaya and Mori, 2005; Favorite, 2017; Raskach, 2009; Nagaya, 2012; Jinaphanh et al., 2016; Kiedrowski, 2017; Yamamoto and Sakamoto, 2019a, 2019b, 2020). The characteristics of these widely used perturbation methods have long been investigated, and the advantages and weaknesses of the methods have been evaluated. The weakness of CS is that it involves an unbounded statistical uncertainty for a large perturbation (Rief, 1984). Meanwhile, DOS is a method that yields the derivative of the flux with respect to a cross section instead of yielding the flux difference. Thus, DOS provides an approximate flux difference by the Taylor series expansion with respect to a cross section. The higher-order derivatives are considered, and more accurate results can be obtained. Thus, while the flux difference can be estimated by lower order derivatives for a small cross section perturbation, accurate estimation for a large perturbation requires a large number of higher-order derivatives.

This paper focuses on fixed-source Monte Carlo perturbation calculations for change in geometry. Perturbation calculations for geometry change are powerful methods for identifying the effect of uncertainties in material size or location. Perturbation due to geometry change can be represented by replacing a material in a perturbed region with the material that occupies the adjoining region beyond the geometry change. The change in geometry of an external boundary where a vacuum boundary condition is imposed is equivalent to the exchange between the vacuum and the outermost material. The cross-section perturbation due to geometry change in most cases may presumably exceed the range of "small perturbation" for which DOS and CS can provide accurate results even if the geometry change itself is small. Therefore, the well-known Monte Carlo perturbation methods, DOS and CS, may not be suitable for calculating the geometry change.

Another robust and exact method for Monte Carlo fixed source perturbation calculations, which is dubbed as "the perturbation source method" (PSM), was formerly proposed by Matthes,

(1972), Preeg and Tsang (1982), and Lux and Koblinger (1991). Although PSM had drawn little interest for decades as a Monte Carlo perturbation method, it was revisited by Sakamoto and Yamamoto (2017) and improved to increase the computational efficiency. The fundamental theory of PSM can be extended to sensitivity analyses in fixed source calculations. PSM is expected to be a Monte Carlo perturbation calculation method that may be applied to geometry change owing to its robustness and efficiency.

Deterministic codes routinely handle sensitivities of estimates with respect to the location of each material interface and the outer boundary (e.g., Favorite and Gonzalez, 2017; Favorite, 2018). As for the Monte Carlo method, some previous researches on geometry change are, for example, (Takahashi, 1970; Kiedrowski and Favorite, 2011; Burke and Kiedrowski, 2018). These Monte Carlo methods aim at the calculation of the first-order derivatives of k_{eff} with respect to system dimensions rather than the change of estimates due to geometry changes. The methods in (Takahashi, 1970; Kiedrowski and Favorite, 2011) need to simulate additional random walks in order to estimate the contributions of system dimension perturbations, which is similar to PSM in terms of requiring additional random walks of "perturbation particles". The method developed in (Burke and Kiedrowski, 2018) circumvents simulating additional random walks by introducing kernel density estimators. The feature of PSM is the capability to provide *exact* flux change by tracking "perturbation particles" that represent the flux difference within the *perturbed* system (Sakamoto and Yamamoto, 2017).

In Section 2, the fundamentals of PSM are revisited, and its application to geometry change is presented. In Section 3, some numerical examples of PSM are presented, and its superiority over other perturbation methods such as CS is exemplified. In Section 4, the applicability of PSM to the perturbation of a fixed source is discussed. A summary and conclusions are provided in Section 5.

2. Theory of perturbation source method

2.1 Transport equation for flux difference due to perturbation

The theory of the perturbation source method (PSM) is briefly reviewed, although it has already been presented in previous publications (e.g., Sakamoto and Yamamoto, 2017). The fixed-source radiation transport equation in a non-multiplying system is given by:

$$\boldsymbol{H}\phi(\boldsymbol{r},\boldsymbol{\Omega},E) = S(\boldsymbol{r},\boldsymbol{\Omega},E), \tag{1}$$

where

$$\boldsymbol{H}\phi(\boldsymbol{r},\boldsymbol{\Omega},E) \equiv \boldsymbol{\Omega}\cdot\boldsymbol{\nabla}\phi(\boldsymbol{r},\boldsymbol{\Omega},E) + \Sigma_t(\boldsymbol{r},E)\phi(\boldsymbol{r},\boldsymbol{\Omega},E) - \int_{4\pi} d\boldsymbol{\Omega}' \int dE' \Sigma_s(\boldsymbol{r},\boldsymbol{\Omega}'\to\boldsymbol{\Omega},E'\to E)\phi(\boldsymbol{r},\boldsymbol{\Omega}',E'), \tag{2}$$

$\phi(\boldsymbol{r},\boldsymbol{\Omega},E) =$ the flux at position $\boldsymbol{r}$ with energy E and direction $\boldsymbol{\Omega}$, $S(\boldsymbol{r},\boldsymbol{\Omega},E) =$ external source term, $\Sigma_t =$ total cross section, and $\Sigma_s =$ scattering cross section. When the cross sections, Σ_t and Σ_s, change to $\Sigma_t + \Delta\Sigma_t$ and $\Sigma_s + \Delta\Sigma_s$, respectively, Eq. (1) changes to

$$(\boldsymbol{H} + \Delta\boldsymbol{H})\big(\phi(\boldsymbol{r},\boldsymbol{\Omega},E) + \delta\phi(\boldsymbol{r},\boldsymbol{\Omega},E)\big) = S(\boldsymbol{r},\boldsymbol{\Omega},E), \tag{3}$$

where

$$\Delta\boldsymbol{H}(\cdots) \equiv \Delta\Sigma_t(\boldsymbol{r},E)(\cdots) - \int_{4\pi} d\boldsymbol{\Omega}' \int dE' \Delta\Sigma_s(\boldsymbol{r},\boldsymbol{\Omega}'\to\boldsymbol{\Omega},E'\to E)(\cdots)\,, \tag{4}$$

where $\delta\phi$ is the flux change due to the changes in cross section. It is assumed that the external source term S is kept constant before and after the perturbation. Subtracting Eq. (1) from Eq. (3) yields the transport equation for $\delta\phi$

$$(\boldsymbol{H} + \Delta\boldsymbol{H})\delta\phi(\boldsymbol{r},\boldsymbol{\Omega},E) = -\Delta\boldsymbol{H}\phi(\boldsymbol{r},\boldsymbol{\Omega},E). \tag{5}$$

The right-hand side of Eq. (5) can be rewritten as

$$-\Delta\boldsymbol{H}\phi(\boldsymbol{r},\boldsymbol{\Omega},E) = -\Delta\Sigma_t(\boldsymbol{r},E)\phi(\boldsymbol{r},\boldsymbol{\Omega},E) + \int_{4\pi} d\boldsymbol{\Omega}' \int dE' \Delta\Sigma_s(\boldsymbol{r},\boldsymbol{\Omega}'\to\boldsymbol{\Omega},E'\to E)\phi(\boldsymbol{r},\boldsymbol{\Omega}',E'). \tag{6}$$

The right-hand side of Eq. (5) is the source term for the transport equation of $\delta\phi$. The flux, ϕ, on the right-hand side is the flux in the unperturbed system. Eq. (5) does not involve any approximation, and the flux change, $\delta\phi$, can be obtained by solving Eq. (5).

2.2 Monte Carlo algorithm of PSM

In a Monte Carlo algorithm proposed by Sakamoto and Yamamoto (2017), the random walk process for solving Eq. (5) is performed for solving Eq. (1) for the fixed-source problem in the unperturbed system. The entire process is composed of two modes: the fixed source mode and the perturbation mode. The Monte Carlo algorithm for solving Eq. (5) is as follows:

(1) The calculation starts with the fixed-source mode for solving Eq. (1). At the beginning of the fixed source mode, a source particle is emitted from the external source according to the source term *S*, and the particle is tracked in the *unperturbed* system.

(2) When the particle undergoes collision in a perturbed region, the random walk process in the fixed source mode is suspended. Then, the calculation mode is switched to the perturbation mode.

(3) As shown in Eq. (6), the source term for the flux difference is composed of two terms. The first is caused by the change in the total cross section. A source particle representing the change in total cross-section (the first term on the right-hand side of Eq. (6)) is emitted from the collision point. The weight of the source particle is given by:

$$W_{\mathrm{t}} = -(\Sigma_t^p - \Sigma_t^{up})\frac{W}{\Sigma_t^{un}}, \tag{7}$$

where W is the weight of the colliding particle in the fixed source mode, and Σ_t^p and Σ_t^{un} are the perturbed and unperturbed total cross sections, respectively. The energy and direction of the source particle are the same as those of the colliding particle. The particle, which is called "perturbation particle" hereafter, is tracked in the *perturbed* system until its death.

(4) The second source term is caused by the change in the scattering cross section, which is represented by the second term on the right-hand side of Eq. (6). The change in the scattering cross section is divided into two components: the change in the total scattering cross section and the change in the collision law. The direction $\boldsymbol{\Omega}'$ and energy E' of the source particle were sampled from the collision law in the *unperturbed* system. The weight of the source particle for the change in the total scattering cross section is given by

$$W_{\mathrm{s}} = (\Sigma_s^p - \Sigma_s^{un})\frac{W}{\Sigma_t^{un}}, \tag{8}$$

where Σ_s^p and Σ_s^{un} are the perturbed and unperturbed total scattering cross-sections, respectively. The weight of the source particle corresponding to the change in the collision law is given by

$$W_{\mathrm{a}} = \frac{f^p(\boldsymbol{\Omega}\cdot\boldsymbol{\Omega}', E \to E') - f^{un}(\boldsymbol{\Omega}\cdot\boldsymbol{\Omega}', E \to E')}{f^{un}(\boldsymbol{\Omega}\cdot\boldsymbol{\Omega}', E \to E')} \Sigma_s^p \frac{W}{\Sigma_t^{un}}, \tag{9}$$

where $f(\boldsymbol{\Omega}\cdot\boldsymbol{\Omega}', E \to E')$ is the probability that the direction and energy after scattering becomes $\boldsymbol{\Omega}'$ and E' from $\boldsymbol{\Omega}$ and E, respectively. The superscript *p* or *un* on *f* denotes that the scattering law belongs to the perturbed or unperturbed system, respectively. In addition to the source particle defined in Eq. (7), another source particle with a weight of $W_{\mathrm{s}} + W_a$ is emitted from the collision point. This perturbation particle is also tracked in the *perturbed* system until its death. Eq. (9) is available on the condition that the ranges of $\boldsymbol{\Omega}\cdot\boldsymbol{\Omega}'$ and E' in the unperturbed system include their entire range in the perturbed system. Thus, voids cannot represent a material in an unperturbed system because $\boldsymbol{\Omega}\cdot\boldsymbol{\Omega}'$ is always unity in a void. The unavailability of voids for a material in an unperturbed system can be circumvented by using a very low density material as an alternative to voids. Meanwhile, a material containing light hydrogen, such as light water, is not available for an unperturbed system because the term $\boldsymbol{\Omega}\cdot\boldsymbol{\Omega}'$ for light hydrogen is not below zero, whereas $\boldsymbol{\Omega}\cdot\boldsymbol{\Omega}'$ of a material that does not contain light hydrogen ranges between −1 and 1. In addition, if PSM is applied in continuous energy Monte Carlo, a nuclide that has a scattering law with a Dirac delta function cannot be contained in an unperturbed system.

(5) After steps (3) and (4) are completed, the calculation mode is returned to the fixed source mode. Then, the fixed source calculation that is suspended in step (2) is resumed.

(6) After the particle that is emitted in step (1) is killed, return to step (1) and another new source particle is emitted.

(7) Steps (1) through (6) are repeated until the desired statistics are obtained.

A flowchart of the PSM is shown in Fig. 1 in (Sakamoto and Yamamoto, 2017). The flux calculated in steps (3) and (4) represents the change in flux $\delta\phi$ due to the perturbation.

2.3 Improvement of PSM efficiency

The efficiency of PSM can be improved by increasing the number of perturbation particles that are emitted in steps (3) and (4), especially when the perturbed region is small and fewer collisions occur in the region. Because the number of perturbation particles is proportional to the number of collisions in the perturbed region, the efficiency can be enhanced by increasing the number of collisions. For this purpose, a pseudo-scattering cross section was added to the perturbed region. The total cross section in the perturbed region is multiplied by a factor of C (>1):

$$\Sigma_t^* = C\Sigma_t, \tag{10}$$

where Σ_t^* is a pseudo-total cross section. The fixed source mode calculation uses Σ_t^* for the total cross section in the perturbed region. The number of perturbation particles that was increased forcibly is compensated for by decreasing the weight of the perturbation particles as follows:

$$W_{\mathrm{t}}^* = \frac{1}{C} W_t, \tag{11}$$

$$W_{\mathrm{s}}^* + W_a^* = \frac{1}{C}(W_s + W_a)\,. \tag{12}$$

After steps (3) and (4) in Section 2.2, a pseudo random number ξ between 0 and 1 is generated. If $\xi < 1/\mathrm{C}$, the collision is accepted as a real collision. Otherwise, the collision is rejected and the particle continues flying without any change in the weight, energy, and direction.

2.4 PSM for geometry change

(1) Displacement of the internal material

In this section, we discuss how PSM treats the geometry change in a fixed source calculation. Fig. 1 shows an example where material 2 is displaced upward within material 1. This change in geometry can be attained by replacing material 1 with material 2 in region 1, and replacing material 2 with material 1 in region 2. For example, when a particle undergoes a collision in region 1 in the fixed source mode calculation, Σ_t^p and Σ_t^{un} in Eq. (7) are the total cross sections of material 2 and material 1, respectively. Similarly, when a particle undergoes a collision in region 2, Σ_t^p and Σ_t^{un} are the total cross sections of material 1 and material 2, respectively.

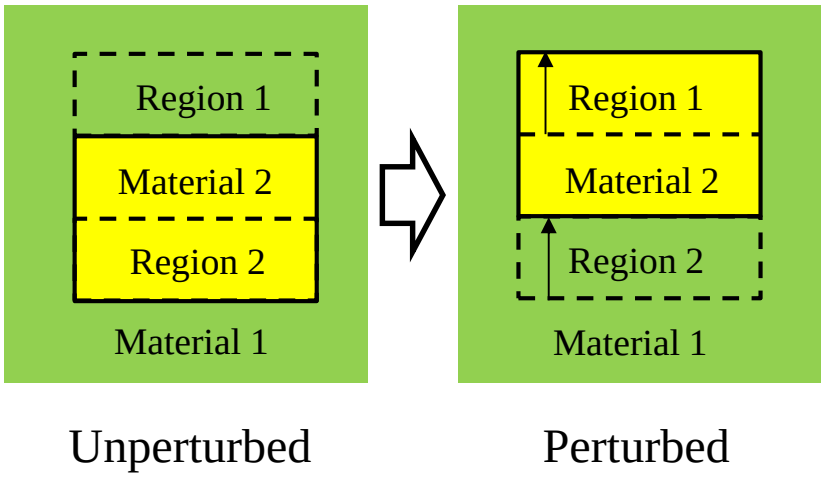

Fig. 1 Upward displacement of the material 2 within material 1.

[Fig. 1]

(2) External boundary changes

The geometry change of an external boundary exposed to vacuum is illustrated in Fig 2, where the upper external boundary recedes downward. This change in geometry is represented by replacing the material in region 1 with a void. If a non-void material is replaced with a void due to the change in geometry, PSM can be performed by setting

$$\Sigma_t^p = \Sigma_s^p = f^p(\boldsymbol{\Omega} \cdot \boldsymbol{\Omega}', E \to E') = 0, \tag{13}$$

in Eqs. (7), (8), and (9). For the reason stated in Section 2.2, voids cannot be replaced with a non-void material without using an alternative very low density material. Therefore, the change in geometry should be done in such a way that the void outside the external boundary is replaced with the material inside the boundary. In other words, the geometry change of an external boundary should be performed in the direction shown in Fig. 2 (from (a) to (b)).

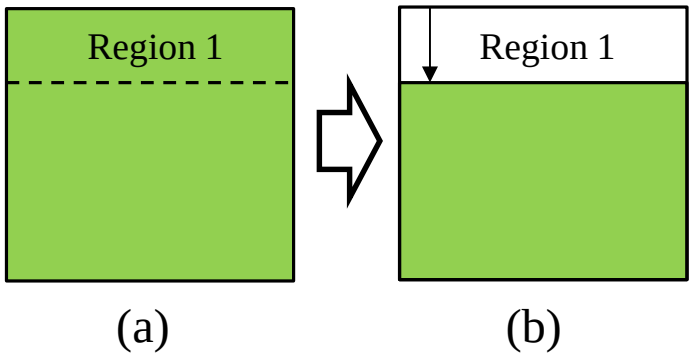

Fig. 2 Replacement of the material in the region 1 with void.

[Fig. 2]

(3) Displacement of internal light water

PSM cannot directly treat the displacement of internal material illustrated in Fig. 1 when the internal material is light water, as already stated in Section 2.2. In such a case, the geometry change can be handled by performing two PSM calculations. First, an unperturbed system is set up by replacing material 2 in region 2 with material 1, as shown in the left part of Fig. 3. The first PSM calculation is performed for a perturbation where material 1 in region 1 is replaced with material 2, as shown in the upper right part of Fig. 3. The second PSM calculation is performed for a perturbation where material 1 in region 2 is replaced with material 2, as shown in the lower right part of Fig. 3. Let $\delta\phi_1$ and $\delta\phi_2$ be flux differences calculated in the first and second PSM calculations, respectively. Then, the flux difference $\delta\phi$ due to the upward displacement of the light water is eventually given by

$$\delta\phi = \delta\phi_1 - \delta\phi_2. \tag{14}$$

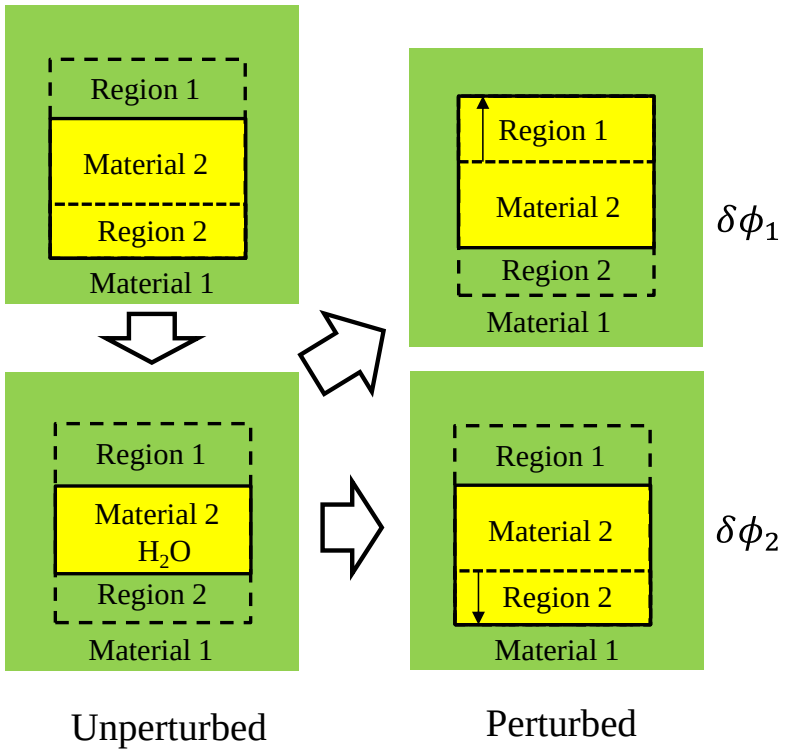

Fig. 3 Displacement of the material 2 made of light water.

[Fig. 3]

3. Numerical tests for geometry changes

3.1 Verification of PSM

Before presenting the results of PSM calculations for geometry change, the verification of PSM is presented for cross section change. All calculations in this study were performed for two-dimensional rectangular geometry. A line neutron beam entered perpendicular to the center of side 4 as shown in Fig. 4. Throughout this paper, the calculations were performed using the three-energy group constants of graphite, 700 ppm borated water, and iron, as shown in Tables 1, 2, and 3, respectively. Anisotropic scattering was considered up to the P_1 order. Scattering cross sections that are not listed in the tables are all zero. The upper and lower energy boundaries of the 2nd-energy group were 6.7 keV and 0.993 eV, respectively. The energy spectrum of the incident beam was $\phi_1 : \phi_2 : \phi_3 =$ 0.343: 0.252: 0.405, which is a neutron spectrum in a light water reactor. The verification calculations were performed for rectangular graphite with a cross section of 2 × 2 cm, as shown in Fig. 4. This unrealistically tiny geometry was chosen to ensure negligibly small statistical uncertainties in the reference solution, which is to be compared with the proposed method. The unperturbed system was composed of pure graphite. The perturbation was made by replacing a 0.6 × 0.7 cm rectangular region with 700 ppm borated light water. The dimensions shown in Fig. 4 were

a = 2 cm, b = 0.9 cm, c = 1.1 cm, d = 0.7 cm, and e = 0.6 cm.

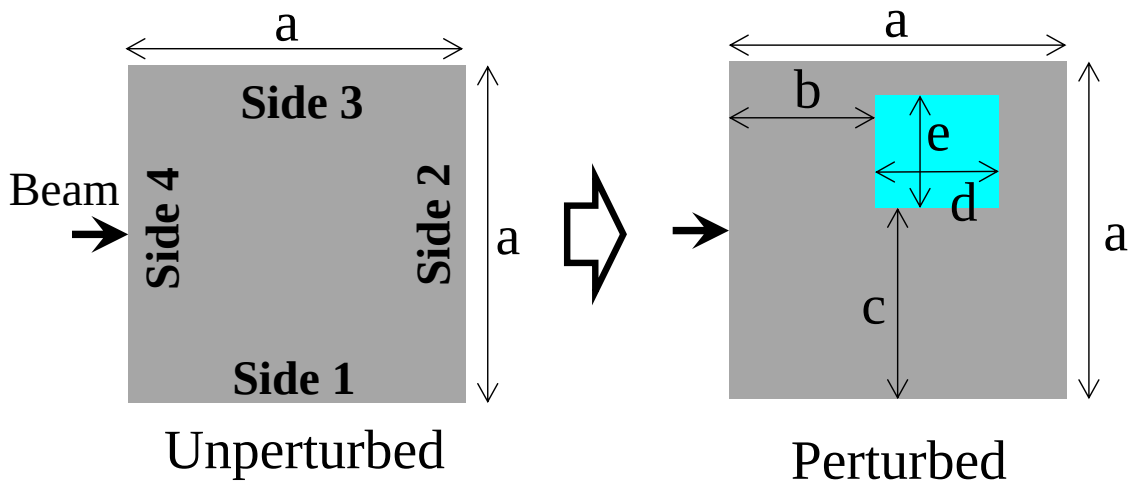

a = 2 cm, b = 0.9 cm, c = 1.1 cm, d = 0.7 cm, e = 0.6 cm.

Fig. 4 Geometry for verification of PSM (not to scale).

[Fig. 4]

The surface fluxes in the 3rd-energy group were calculated for the four external boundaries. Each time a particle escaped one of the four sides, the estimate of the surface flux on each side, $W/(\boldsymbol{n}\cdot\boldsymbol{\Omega})$, was calculated, where $W=$ weight of the particle, $\boldsymbol{\Omega}=$ direction vector of the particle, and $\boldsymbol{n}$ = the unit outward vector normal to the external boundary. The surface flux on side j (=1, 2, 3, and 4) is estimated as follows:

$$S_j = \frac{1}{M}\sum_i \frac{W_i}{\boldsymbol{n}_j\cdot\boldsymbol{\Omega}_i}, \tag{15}$$

where $W_i=$ the ith particle's weight escaping side j, i is summed over all particles escaping side j, and M is the total number of source neutrons. In the calculation of the PSM, W_i is the weight of the perturbation particle and S_j stands for the flux difference due to perturbation. The reference solution was obtained by the difference of the surface fluxes between two independent calculations before and after perturbation, which is dubbed as the "direct" method hereafter.

For the comparison of PSM with another conventional Monte Carlo perturbation method, the correlated sampling method (CS) was applied to the problems in this study. In CS, particles of the perturbed history are forced to follow the same trajectories as the unperturbed history in phase space. The weight of the perturbed history in the CS was estimated at each collision in the perturbed region as

$$W_p' = W_p\cdot exp\left(-\left(\Sigma_t^p-\Sigma_t^{up}\right)s\right)\frac{\Sigma_s^p}{\Sigma_t^{un}}\cdot\frac{f^p(\boldsymbol{\Omega}\cdot\boldsymbol{\Omega}', E\rightarrow E')}{f^{un}(\boldsymbol{\Omega}\cdot\boldsymbol{\Omega}', E\rightarrow E')}, \tag{16}$$

where $W_p=$ the weight of the perturbed history before collision and s is the track length in the perturbed region. The surface flux difference by CS was estimated in the same manner as in Eq. (15):

$$\delta S_j = \frac{1}{M}\sum_i \frac{(W_{p,i}-W_{un,i})}{\boldsymbol{n}_j\cdot\boldsymbol{\Omega}_i}, \tag{17}$$

where $W_{p,i}$ and $W_{un,i}$ are the ith particle weight of the perturbed and unperturbed histories,

respectively. The flux differences on sides 1, 2, and 3 calculated with PSM and CS are compared with the reference solution in Table 4. The CPU times required for the calculations on a single 3.40 GHz CPU are also shown in Table 4. Throughout this paper, all statistical uncertainties are one standard deviation, which are shown in parentheses in each table. The results of the PSM in Table 4 were obtained using the factor defined by Eq. (10), C =1. Table 4 shows that the flux differences calculated with the PSM agree precisely with the references. The results of the CS agree with the references within the statistical uncertainties. However, the agreement of CS with the references is not satisfactory, which is caused by the large statistical uncertainties in CS. Table 5 compares the relative figure-of-merit (FOM) defined by

$$FOM = \frac{1}{\sigma^2 T}, \tag{18}$$

where σ = one standard deviation of absolute uncertainty and T is the computation time. In terms of FOM, PSM is less effective than the direct method (two independent runs) even if the factor C is increased up to 100. The perturbed region of this problem occupies approximately 10% of the entire domain, which is considered relatively large for a perturbed region. Thus, many perturbation particles were emitted from the perturbed region. CS is much less effective than PSM. It can thus be concluded that PSM can yield accurate results for flux differences, though it is not always an efficient method depending on the occupancy rate of a perturbed region.

[Tables 1, 2, 3, 4, 5]

The next example dealt with a perturbation where a void region within graphite was filled with graphite. The perturbation was performed in the reverse direction to that in Fig. 4. As stated in Section 2.2, a complete void region cannot be used as the perturbed region. Then, a very low density material was used instead of void. The total cross sections of the low density material were 5×10^{-4} cm^{-1} and the capture cross sections were zero for all energy groups. The scattering was isotropic. The flux differences on sides 1, 2, and 3 calculated with PSM and CS are compared with the reference solution in Table 6. Table 7 compares the relative FOMs. The results of PSM agree well with the references. However, the efficiency of PSM with C =1 is far inferior to the direct method because the collisions rarely occur in the low density material and the perturbation

particles are not sufficiently emitted from the perturbed region. The inferior efficiency can be improved by increasing *C*, which increases pseudo scatterings and perturbation particles. The results of CS in Table 6 suggests that CS is not necessarily unavailable but unsuitable for this problem.

[Tables 6, 7]

3.2 Displacement of internal borated water in graphite

PSM was applied to a 20 × 20 cm rectangular graphite that includes a 1 × 2 cm internal borated light water region, as shown in Fig. 5. A change in geometry was induced by displacing the internal borated light water upward by 0.05 cm. The dimensions in Fig 5 were

a = 20 cm, b = 9 cm, c = 1 cm, d = 2 cm, and e = 0.05 cm.

Because this problem includes light water, PSM calculations were performed in two steps, as shown in Fig. 3. In CS, light water cannot be replaced with another material in the same manner as in PSM, while material replacement in the inverse direction is possible. Thus, CS calculations were also performed using the same procedure as for PSM. The flux differences on the two surfaces, sides 1 and 3, and the relative FOMs are shown in Tables 8 and 9, respectively. The results for side 2 are omitted because the flux difference on side 2 was negligibly small. Table 8 shows that the direct method and CS can no longer yield statistically significant results for this small displacement. The computational efficiency of PSM without pseudo scattering (i.e., $C = 1$) is equivalent to the direct method. On the other hand, the fractional standard deviation of PSM with $C = 500$ is less than 3%, suggesting that PSM with the pseudo scattering method is an exclusively available calculation method for this small perturbation. As shown in Table 9, the computational efficiency of the PSM is improved with an increase in the factor *C* within the range of this numerical test.

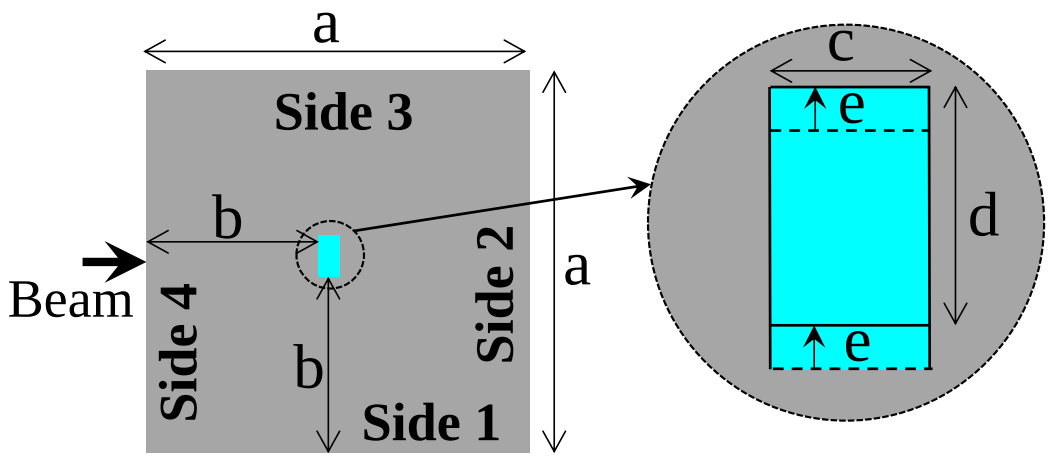

a = 20 cm, b = 9 cm, c = 1 cm , d = 2 cm, e = 0.05 cm.

Fig. 5 Geometry of slight displacement of internal material (light water or iron) (not to scale).

[Fig. 5] [Tables 8, 9]

3.3 Displacement of internal iron in graphite

This section deals with the same geometry change as in Section 3.2, but the internal material is iron. Unlike in the previous section, two-step calculations are not necessary. The PSM and CS calculations can be performed only once according to the procedure shown in Fig. 1. The flux differences calculated with the direct method, PSM, and CS are shown in Table 10. The relative FOMs are listed in Table 11. The statistical uncertainties of the direct method and CS are much smaller in this problem compared with the previous problem. The FOMs of the PSM are larger than those of the direct method by a factor of thousands. The superiority of PSM to the direct method is more evident in this problem. Although the FOM of CS is smaller than that of PSM by a factor of tens, CS is also an available perturbation method for this problem.

[Tables 10, 11]

3.4 Verification of PSM for external boundary change

A verification calculation of the PSM for an external boundary change was performed again for a 2 × 2 cm graphite. In the perturbed system, a relatively large rectangular region near the beam source was removed from side 4, as shown in Fig. 6. The dimensions of the calculation shown in Fig. 6 were:

a = 2 cm, b = 0.7 cm, c = 0.5 cm, and d = 0.2 cm.

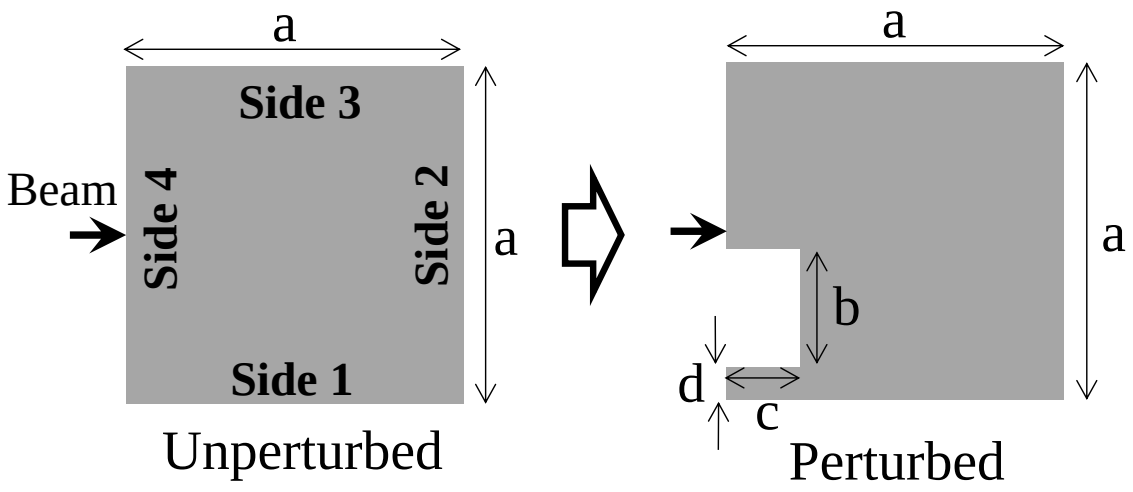

a = 2 cm, b = 0.7 cm, c = 0.5 cm, d= 0.2 cm

Fig. 6 Large change in external boundary (not to scale).

[Fig. 6]

The flux differences on sides 1, 2, and 3 calculated with PSM (C = 1) and CS are compared with the reference solution in Table 12. The flux differences calculated with the three methods agree precisely with each other. The two Monte Carlo perturbation methods, PSM and CS, can yield accurate results for the change in external boundary.

[Table 12]

3.5 Small external boundary change

PSM and CS were applied to an external boundary change in a 20 × 20 cm graphite from which a 0.5 × 0.5 cm rectangular region was removed from side 4, as shown in Fig. 7. The dimensions of the calculation are shown in Fig. 7. The flux differences on sides 1, 2, and 3 calculated with the direct method, PSM, and CS are shown in Table 13. The results calculated with the three methods agree with each other within the statistical uncertainties. The relative FOMs of the three methods are compared in Table 14. The FOMs of the PSM and CS are both much higher than that of the direct method. While CS is a Monte Carlo perturbation method that is applicable to an external boundary change, PSM outperforms CS by a factor of tens or hundreds for this problem.

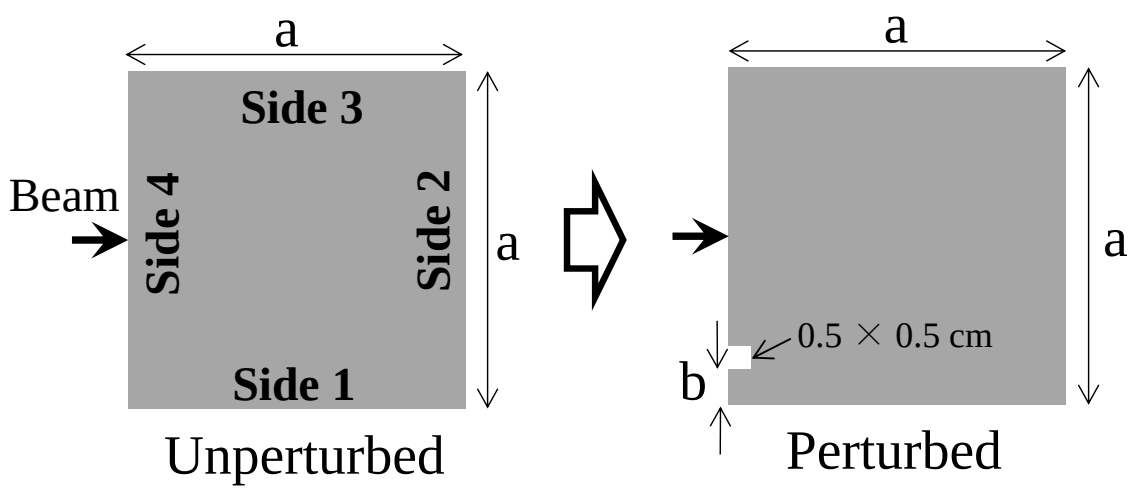

Fig. 7 Small change of external boundary (not to scale).

[Fig. 7] [Tables 13, 14]

4. Perturbation of external source

Eq. (5), the transport equation for $\delta\phi$, is derived under the assumption that the external source is constant before and after perturbation. This section discusses how to deal with the perturbation of the external source. If the cross sections are unchanged before and after the perturbation, the flux change due to the changes in the external source is given by

$$\boldsymbol{H}\delta\phi(\boldsymbol{r},\boldsymbol{\Omega},E) = \Delta S(\boldsymbol{r},\boldsymbol{\Omega},E), \tag{19}$$

where ΔS is the difference of the external source due to the perturbation. The perturbation calculation cannot be performed for the displacement of a point source because $\Delta S(\boldsymbol{r},\boldsymbol{\Omega},E)$ is simply written as

$$\Delta S(\boldsymbol{r},\boldsymbol{\Omega},E) = S(\boldsymbol{\Omega},E)\delta\left(\boldsymbol{r}-\boldsymbol{r}_p\right) - S(\boldsymbol{\Omega},E)\delta(\boldsymbol{r}-\boldsymbol{r}_{un}), \tag{20}$$

where $\boldsymbol{r}_{un}$ and $\boldsymbol{r}_p$ are the positions of the point source before and after the perturbation, respectively. Eq. (20) means that two independent fixed source calculations are required for the displacement of the point source. On the other hand, if the external source is a volume source and the volume source region overlaps before and after the displacement, $\Delta S(\boldsymbol{r},\boldsymbol{\Omega},E)$ is given by

$$\Delta S(\boldsymbol{r},\boldsymbol{\Omega},E) = S(\boldsymbol{\Omega},E)P(\boldsymbol{r}) - S(\boldsymbol{\Omega},E)U(\boldsymbol{r}), \tag{21}$$

where $U(\boldsymbol{r})$ and $P(\boldsymbol{r})$ are the volume source regions where the overlapping region is excluded from the volume source region before and after the displacement, respectively, as shown in Fig. 8.

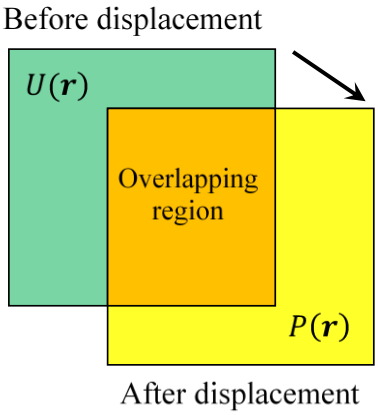

Fig. 8 Displacement of volume source region.

Using Eqs. (19) and (21), the calculation for the source particles emitted from the overlapping region can be omitted. The efficiency with this perturbation method increases with the fraction of the overlapping region.

For perturbation in the angular distribution and energy spectrum of a fixed source, the source term for the transport equation, $\Delta S(\boldsymbol{r},\boldsymbol{\Omega},E)$, is given by

$$\Delta S(\boldsymbol{r},\boldsymbol{\Omega},E) = S(\boldsymbol{r},\boldsymbol{\Omega},E)\frac{f^{p}(\boldsymbol{\Omega},E)-f^{un}(\boldsymbol{\Omega},E)}{f^{un}(\boldsymbol{\Omega},E)}, \tag{22}$$

where $f^{un}(\boldsymbol{\Omega},E)$ and $f^{p}(\boldsymbol{\Omega},E)$ are the probability densities of the angular and energy of the fixed source before and after the perturbation, respectively. However, this method is equivalent to the correlated sampling method. The source particle in the perturbed history of the correlated sampling method is given by

$$S^{p}(\boldsymbol{r},\boldsymbol{\Omega},E) = S(\boldsymbol{r},\boldsymbol{\Omega},E)\frac{f^{p}(\boldsymbol{\Omega},E)}{f^{un}(\boldsymbol{\Omega},E)}. \tag{23}$$

The correlated sampling method calculates the flux difference by subtracting the perturbed flux that is calculated with the perturbed source $S^{p}(\boldsymbol{r},\boldsymbol{\Omega},E)$ in Eq. (23) from that of the unperturbed history. This is eventually identical to the flux difference obtained by using Eqs. (19) and (22).

5. Conclusions

From the numerical tests, it can be concluded that the perturbation source method (PSM) and the correlated sampling method (CS) are Monte Carlo perturbation methods that are available for handling geometry changes in fixed source calculations. PSM is not always suitable for a large geometry change because too many perturbation sources must be emitted from the perturbed

region. When the geometry change is large, PSM is less effective than the two independent runs before and after perturbation. On the other hand, PSM is the most effective Monte Carlo method for small geometry changes. The efficiency of the PSM is optimized by adjusting a pseudo-scattering cross section in the perturbed region. PSM, in particular, is an exclusively available method for a small displacement of internal light water within the surrounding material. PSM and CS can both perform perturbation calculations for the displacement of internal light water using a two-step procedure. Perturbation calculations for external boundary changes can be performed by replacing the material facing the external boundary with a void. PSM and CS are both applicable to external boundary changes. Regardless of the type of geometry change, PSM always outperforms CS in terms of computational efficiency within the range of the numerical tests performed in this study.

References

Bernnat, W., 1974. A Monte Carlo technique for local perturbations in multiplying systems, Proc. NEACRP Specialist Mtg., ANL-75-2, 261 (1974).

Burke, T.P., Kiedrowski, B.C., 2018. Monte Carlo perturbation theory estimates of sensitivities to system dimensions. Nucl. Sci. Eng. 189, 199–223. https://doi.org/10.1080/00295639.2017.1388093.

Densmore, J. D., McKinney, G.W., Hendricks, J.S., 1997. Correction to the MCNP perturbation feature for cross-section dependent tallies, LA-13374.

Favorite, J.A., 2017. Using the MCNP Taylor series perturbation feature (efficiently) for shielding problems. European Physics Journal—Web of Conferences 153, 06030. https://doi.org/10.1051/epjconf/201715306030.

Favorite, J.A., Gonzalez, E., 2017. Revisiting boundary perturbation theory for inhomogeneous transport problems. Nucl. Sci. Eng. 185, 445–459. https://doi.org/10.1080/00295639.2016.1277108.

Favorite J.A., 2018. SENSMG: first-order sensitivities of neutron reaction rates, reaction-rate

ratios, leakage, k_{eff}, and α using PARTISN. Nucl. Sci. Eng. 192, 80–114. https://doi.org/10.1080/00295639.2018.1471296.

He, T., Su, B., 2010. On using correlated sampling to simulate small changes in system response by MCNP, Ann. Nucl. Energy 37, 34–42. https://doi.org/10.1016/j.anucene.2009.10.006.

He, T., Su, B., 2011. Comparison between correlated sampling and the perturbation technique of MCNP5 for fixed-source problems, Ann. Nucl. Energy 38, 1318–1326. https://doi.org/10.1016/j.anucene.2011.02.006.

Jinaphanh, A., Leclaire, N., Cochet, B., 2016. Continuous-energy sensitivity coefficients in the MORET code, Nucl. Sci. Eng. 184, 53–68. https://doi.org/10.13182/NSE16-2.

Kiedrowski, B.C., Favorite, J.A, Brown, F.B., 2011. Monte Carlo calculations of eigenvalue sensitivities to system dimensions," Proc. 9th International Conference on Nuclear Criticality Safety (ICNC2011), Edinburgh, Scotland, UK, Sep. 19–22 (2011). (LA-UR-11-04199 https://laws.lanl.gov/vhosts/mcnp.lanl.gov/pdf_files/la-ur-11-04199.pdf)

Kiedrowski, B.C., 2017. Review of early 21st-century Monte Carlo perturbation and sensitivity techniques for *k*-eigenvalue radiation transport calculations. Nucl. Sci. Eng. 185, 426–444. https://doi.org/10.1080/00295639.2017.1283153.

Lux, I., Koblinger, L., 1991. Monte Carlo Particle Transport Methods: Neutron and Photon Calculations, CRC Press.

McKinney, G.W., Iverson, J.L., 1996. Verification of the Monte Carlo differential operator technique for MCNP, Los Alamos National Laboratory, LA-13098.

Matthes, W., 1972. Calculation of reactivity perturbations with the Monte Carlo method, Nucl. Sci. Eng. 47, 234–237. https://doi.org/10.13182/NSE72-A22403.

Nagaya, Y., Mori, T., 2005. Impact of perturbed fission source on the effective multiplication factor in Monte Carlo perturbation calculations, J. Nucl. Sci. Technol., 42, 428–441. https://doi.org/10.1080/18811248.2005.9726411.

Nagaya, Y., 2012. Doctoral dissertation, Kyoto University (in Japanese) (The title translated from

Japanese is “Study on reactor core analyses by the stochastic method”).

Nakagawa, M., Asaoka T., 1978. Improvement of correlated sampling Monte Carlo Methods for reactivity calculations, J. Nucl. Sci. Technol. 15, 400–410.

Preeg, W.E., Tsang, J.S.K., 1982. Comparison of correlated Monte Carlo techniques, Trans. Am. Nucl. Soc. 43, 628–629.

Raskach, K. F., 2009. An improvement of the Monte Carlo generalized differential operator method by taking into account first- and second-order perturbations of fission source, Nucl. Sci. Eng. 162, 158–166. https://doi.org/10.13182/NSE162-158.

Rief, H., 1984. Generalized Monte Carlo perturbation algorithms for correlated sampling and a second-order Taylor series approach. Ann. Nucl. Energy 9, 455–476. https://doi.org/10.1016/0306-4549(84)90064-1.

Sakamoto, H., Yamamoto, T., 2017. Improvement and performance evaluation of the perturbation source method for an exact Monte Carlo perturbation calculation in fixed source problems, J. Compt. Phys. 345, 245–259. https://doi.org/10.1016/j.jcp.2017.05.004.

Spanier, J., Gelbard, E.M., 1969. Monte Carlo principles and neutron transport problems, Addison-Wesley Publishing Company.

Takahashi, H., 1970. Monte Carlo method for geometrical perturbation and its application to the pulsed fast reactor. Nucl. Sci. Eng. 41, 259–270. https://doi.org/10.13182/NSE70-A20712.

Yamamoto, T., Sakamoto, H., 2019a. A Monte Carlo technique for sensitivity analysis of alpha-eigenvalue with the differential operator sampling method. Ann. Nucl. Energy 127, 178–187. https://doi.org/10.1016/j.anucene.2018.12.012.

Yamamoto, T., Sakamoto, H., 2019b. Two-step Monte Carlo sensitivity analysis of alpha- and gamma-eigenvalues with the differential operator sampling method. Ann. Nucl. Energy 133, 100–109. https://doi.org/10.1016/j.anucene.2019.05.013.

Yamamoto, T., Sakamoto, H., 2020. Monte Carlo sensitivity analysis method for the effective delayed neutron fraction with the differential operator sampling method. Ann. Nucl. Energy

140, 107108. https://doi.org/10.1016/j.anucene.2019.107108.

List of figures

Figure

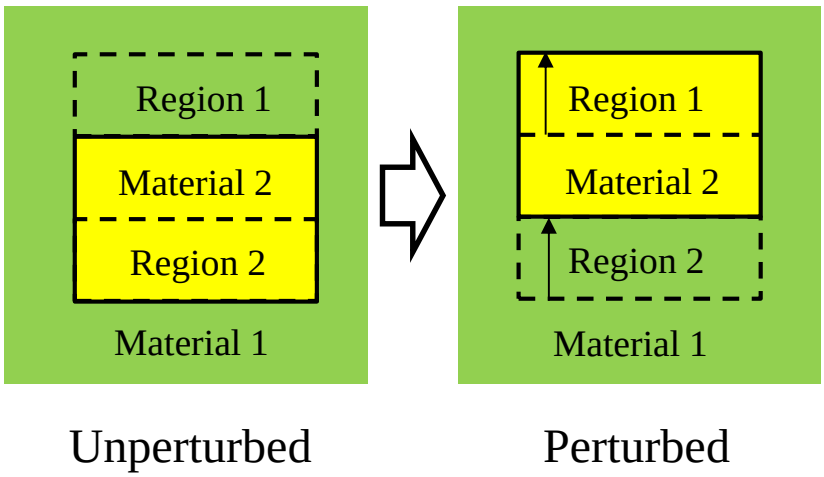

Fig. 1 Upward displacement of material 2 within material 1.

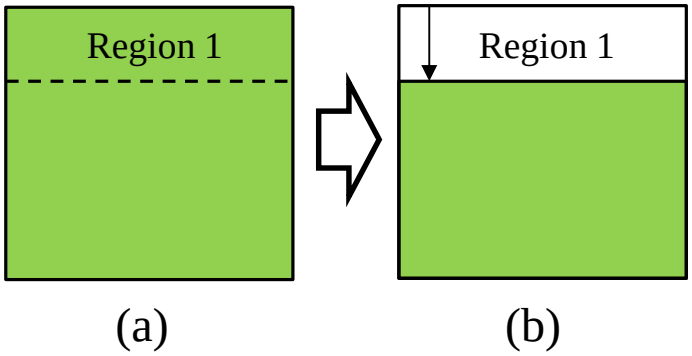

Fig. 2 Replacement of the material in region 1 with void.

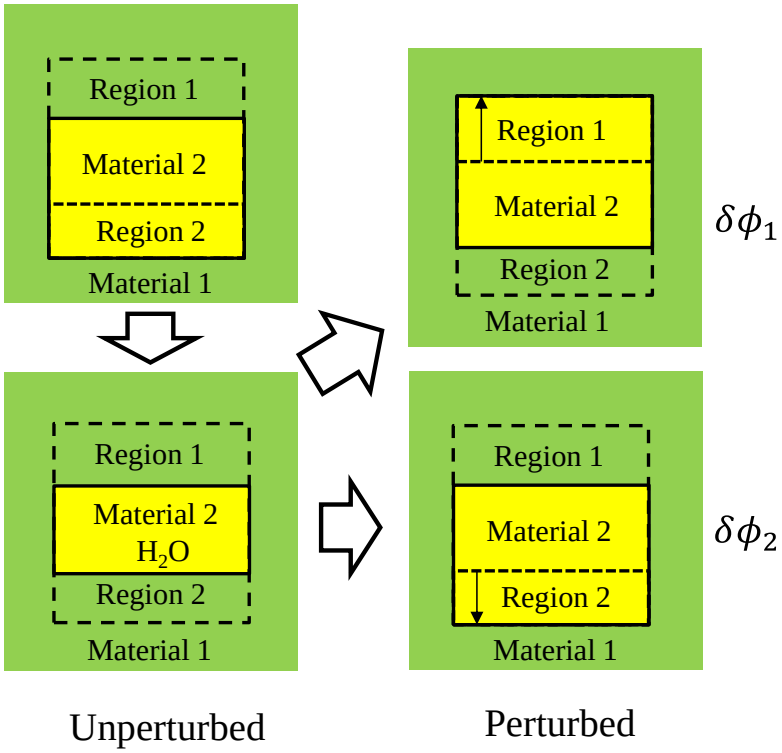

Fig. 3 Displacement of material 2 made of light water.

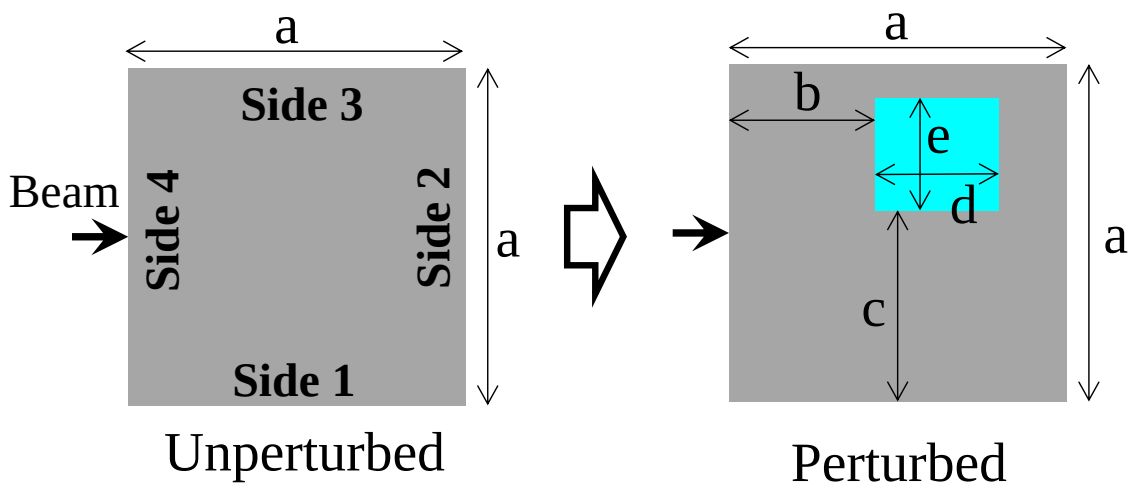

a = 2 cm, b = 0.9 cm, c = 1.1 cm, d = 0.7 cm, e = 0.6 cm.

Fig. 4 Geometry for verification of PSM (not to scale).

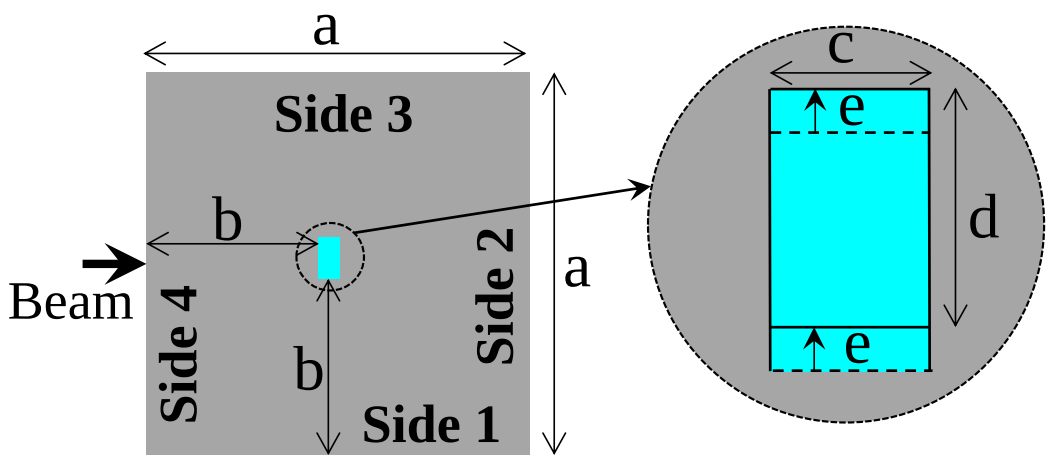

a = 20 cm, b = 9 cm, c = 1 cm , d = 2 cm, e = 0.05 cm.

Fig. 5 Geometry of slight displacement of internal material (light water or iron) (not to scale).

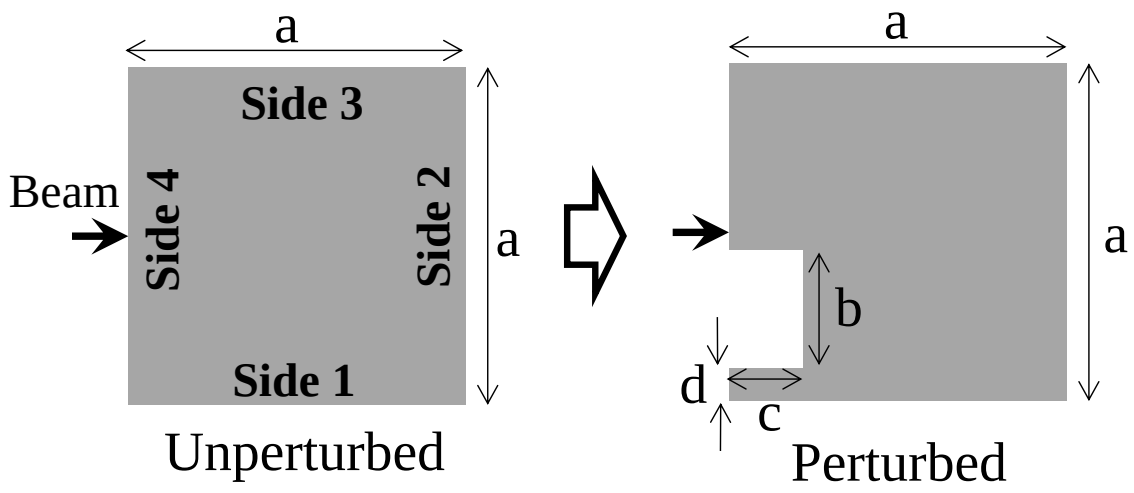

a = 2 cm, b = 0.7 cm, c = 0.5 cm, d= 0.2 cm

Fig. 6 Large change of external boundary (not to scale).

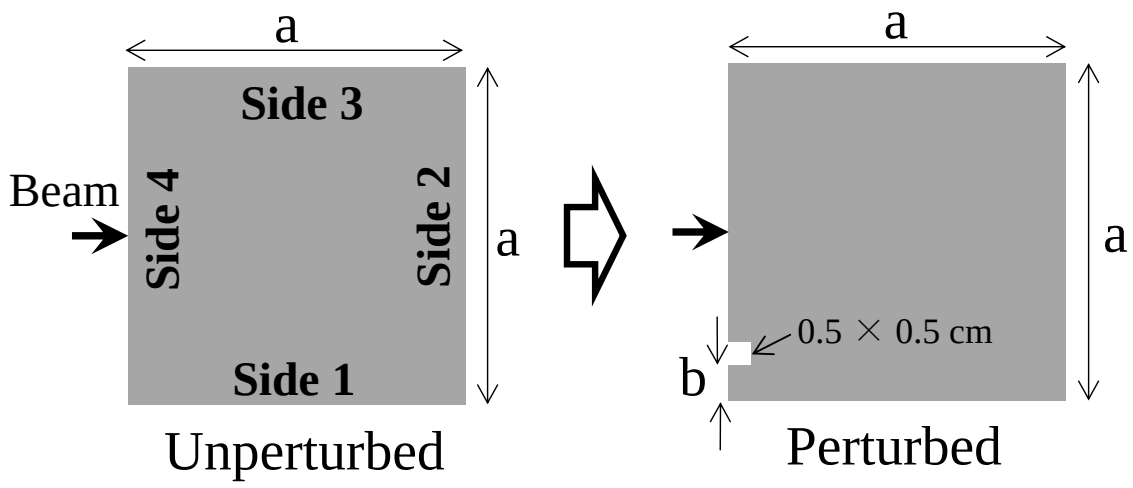

Fig. 7 Small change of external boundary (not to scale).

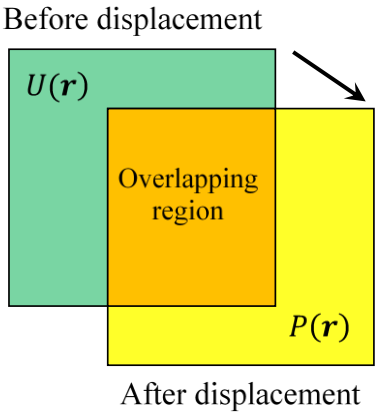

Fig. 8 Displacement of volume source region.

Table

Table 1 Three group constants of graphite.

	1st group (10 MeV~67 keV)	2nd group (67 keV~0.993 eV)	3rd group (0.993 eV~)
Σ_t (cm^{-1})	2.3264E-1*	4.1793E-1	4.2354E-1
Σ_c (cm^{-1})	4.1681E-5	7.6738E-6	2.1311E-4
$\Sigma_{s0g\to g}$ (cm^{-1})**	2.2122E-1	4.1327E-1	2.5313E+0
$\Sigma_{s1g\to g}$ (cm^{-1}) ***	7.1347E-2	2.5455E-2	4.7530E-3
$\Sigma_{s0g\to g+1}$ (cm^{-1}) **	1.1379E-2	4.6514E-3	—
$\Sigma_{s1g\to g+1}$ (cm^{-1}) ***	-1.2324E-2	-1.3671E-3	—

*Read as 2.3264×10^{-1}, **P_0 component, ***P_1 component

Table 2 Three group constants of 700 ppm borated water.

	1st group (10 MeV~67 keV)	2nd group (67 keV~0.993 eV)	3rd group (0.993 eV~)
Σ_t (cm^{-1})	4.0767E-1*	1.3898E+0	2.6785E+0
Σ_c (cm^{-1})	2.2521E-4	1.4719E-3	4.1358E-2
$\Sigma_{s0g\to g}$ (cm^{-1})**	3.1343E-1	1.2638E+0	2.6372E+0
$\Sigma_{s1g\to g}$ (cm^{-1}) ***	2.4187E-1	8.4735E-1	1.1204E+0
$\Sigma_{s0g\to g+1}$ (cm^{-1}) **	9.4022E-2	1.2447E-1	—
$\Sigma_{s1g\to g+1}$ (cm^{-1}) ***	2.5721E-2	4.3228E-2	—

*Read as 4.0767×10^{-1}, **P_0 component, ***P_1 component

Table 3 Three group constants of iron.

	1st group (10 MeV~67 keV)	2nd group (67 keV~0.993 eV)	3rd group (0.993 eV~)
Σ_t (cm^{-1})	2.3126E-1*	5.1427E-1	1.0817E+0
Σ_c (cm^{-1})	4.0473E-4	4.0303E-3	9.6042E-2
$\Sigma_{s0g\to g}$ (cm^{-1})**	2.2908E-1	5.0902E-1	9.8568E-1
$\Sigma_{s1g\to g}$ (cm^{-1}) ***	3.5682E-2	1.0585E-1	-7.7815E-3
$\Sigma_{s0g\to g+1}$ (cm^{-1}) **	1.7711E-3	1.2159E-3	—
$\Sigma_{s1g\to g+1}$ (cm^{-1}) ***	-1.9989E-4	-4.6385E-4	—

*Read as 2.3126×10^{-1}, **P_0 component, ***P_1 component

Table 4 Difference of the surface fluxes due to replacement of graphite with light water

	Side 1	Side 2	Side 3	CPU time (min)
Direct	6.92E−2[a] (7E−6)	−6.39E−2 (1E−5)	4.19E−2 (7E−6)	124
PSM (C=1)	6.92E−2 (6E−5)	−6.39E−2 (8E−5)	4.18E−2 (6E−5)	16
CS	6.78E−2 (4E−4)	−6.10E−2 (4E−3)	4.22E−2 (2E−3)	55

[a] Read as 6.92×10^{-2}

Table 5 Relative figure-of-merit for the results of Table 4.

	Side 1	Side 2	Side 3
Direct	1	1	1
PSM (C=1)	0.124	0.127	0.118
PSM (C=10)	0.197	0.194	0.182
PSM (C=100)	0.244	0.181	0.199
CS	7.79E−4[a]	1.65E−5	4.01E−5

[a] Read as 7.79×10^{-4}

Table 6 Difference of the surface fluxes due to replacement of void with graphite

	Side 1	Side 2	Side 3	CPU time (min)
Direct	2.60E−2[a] (5E−6)	−3.90E−2 (1E−5)	2.35E−2 (5E−6)	96
PSM (C=1)	2.59E−2 (1E−4)	−3.90E−2 (2E−4)	2.34E−2 (1E−4)	32
PSM (C=100)	2.59E−2 (9E−6)	−3.89E−2 (1E−5)	2.34E−2 (9E−6)	54
PSM (C=1000)	2.59E−2 (4E−6)	−3.89E−2 (7E−6)	2.34E−2 (5E−6)	41
CS	2.41E−2 (6E−4)	−4.13E−2 (7E−4)	2.12E−2 (7E−4)	29

[a] Read as 2.60×10^{-2}

Table 7 Relative figure-of-merit for the results of Table 6.

	Side 1	Side 2	Side 3
Direct	1	1	1
PSM (C=1)	8.93E−3[a]	1.04E−2	6.63E−3
PSM (C=100)	0.697	0.891	0.609
PSM (C=1000)	3.69	4.61	3.22
CS	3.14E−4	7.25E−4	1.82E−4

[a] Read as 8.93×10^{-3}

Table 8 Difference of the surface fluxes due to displacement of light water in graphite

	Side 1	Side 3	CPU time (min)
Direct	1.60E−5[a] (1.05E−5)	−2.12E−6 (1.05E−5)	461
PSM (C = 500)	2.54E−5 (7E−7)	−2.57E−5 (7E−7)	452
CS	5.98E−5 (1.36E−5)	−2.29E−5 (1.29E−5)	340

[a] Read as 1.60×10^{-5}

Table 9 Relative figure-of-merit for the results of Table 8.

	Side 1	Side 3
Direct	1	1
PSM (C=1)	2.88	2.82
PSM (C=100)	130	126
PSM (C=300)	178	187
PSM (C=500)	208	211
PSM (C=1000)	223	218
CS	0.804	0.900

Table 10 Difference of the surface fluxes due to displacement of iron in graphite.

	Side 1	Side 3	CPU time (min)
Direct	5.20E−5[a] (6.4E−6)	−4.80E−5 (6.4E−6)	1122
PSM (C = 100)	4.59E−5 (2E−7)	−4.53E−5 (2E−7)	336
CS	4.54E−5 (7E−7)	−4.66E−5 (7E−7)	270

[a] Read as 5.20×10^{-5}

Table 11 Relative figure-of-merit for the results of Table 10.

	Side 1	Side 3
Direct	1	1
PSM (C=1)	240	195
PSM (C=100)	5.52E+3[a]	4.51E+3
PSM (C=500)	6.95E+3	5.66E+3
PSM (C=1000)	7.05E+3	5.78E+3
CS	419	379

[a] Read as 5.52×10^{3}

Table 12 Difference of the surface fluxes due to large external boundary change.

	Side 1	Side 2	Side 3	CPU time (min)
Direct	2.42E−3[a] (6E−6)	−1.81E−3 (1E−5)	−2.40E−3 (6E−6)	95
PSM (C = 1)	2.43E−3 (4E−6)	−1.81E−3 (2E−6)	−2.40E−3 (2E−6)	11
CS	2.42E−5 (7E−6)	−1.81E−3 (1E−6)	−2.39E−3 (1E−6)	31

[a] Read as 2.42×10^{-3}

Table 13 Difference of the surface fluxes due to small external boundary change.

	Side 1	Side 2	Side 3	CPU time (min)
Direct	−2.26E−4[a] (1.2E−5)	−1.75E−5 (8.9E−6)	−7.49E−6 (1.2E−5)	308
PSM (C=500)	−2.28E−4 (1E−7)	−1.81E−5 (1E−8)	−1.92E−5 (1E−8)	58
CS	−2.29E−4 (9E−7)	−1.80E−5 (2E−7)	−1.94E−5 (3E−7)	56

[a] Read as -2.26×10^{-4}

Table 14 Relative figure-of-merit for the results of Table 13.

	Side 1	Side 2	Side 3
Direct	1	1	1
PSM (C=1)	836	5.84E+3	1.73E+4
PSM (C=100)	3.35E+4 [a]	7.21E+5	1.21E+6
PSM (C=300)	4.11E+4	1.77E+6	2.85E+6
PSM (C=500)	3.92E+4	2.44E+6	3.84E+6
PSM (C=1000)	3.13E+4	3.23E+6	5.10E+6
CS	942	1.01E+4	1.07E+4

[a] Read as 3.35×10^{4}

Declaration of interest statement

The authors declare no conflicts of interest associated with this manuscript.

Graphical Abstract

An accurate Monte Caro perturbation method for fixed source calculations has been developed for small geometry change as shown below.

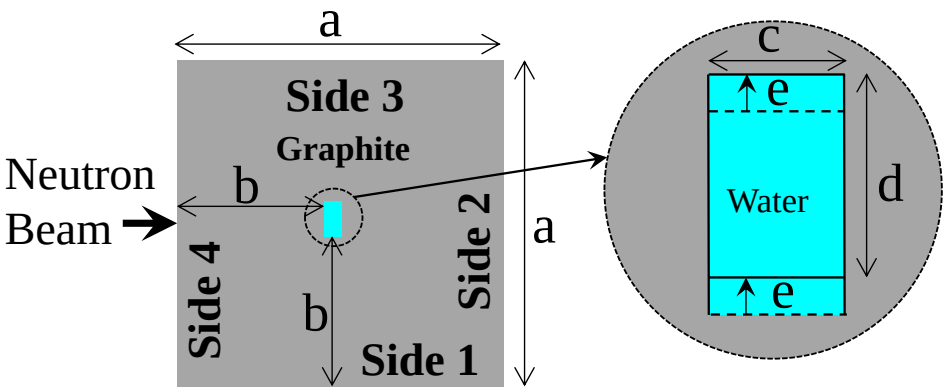

a = 20 cm, b = 9 cm, c = 1 cm , d = 2 cm, e = 0.05 cm.

The perturbation source method (PSM), which is a Monte Carlo perturbation calculation method, is applied to geometry changes in fixed-source neutron transport problems. In PSM, perturbation particles that represent the flux difference due to the changes in geometry are explicitly tracked within the perturbed system. A perturbation calculation for geometry change can be performed by replacing the material in a perturbed region with the material that occupies the adjoining region beyond the geometry change. The efficiency of the PSM can be enhanced by adding a pseudo-scattering cross section to the perturbed region. For geometry changes where the perturbed region is small, PSM exhibits excellent performance compared to the two independent runs before and after the perturbation if optimized pseudo-scattering cross sections are used. This method can also be applied to perturbation due to an external boundary change. Although the correlated sampling method (CS) is another available Monte Carlo method for geometry change, PSM largely outperforms CS in terms of computational efficiency for the numerical examples tested in this study.

Monte Carlo perturbation calculation for geometry change in fixed source problems with the perturbation source method

Toshihiro Yamamoto
Institute for Integrated Radiation and Nuclear Science, Kyoto University, 2 Asashiro Nishi, Kumatori-cho, Sennan-gun, Osaka, 590-0494, Japan

Hiroki Sakamoto
Radiation Dose Analysis and Evaluation Network, 4-13-14, Kokubunji-shi, Tokyo, 185-0001, Japan

CRediT authorship contribution statement

Toshihiro Yamamoto: Supervision, Methodology, Conceptualization, Investigation, Writing - original draft. **Hiroki Sakamoto**: Software, Validation, Formal analysis, Data curation, Writing - review & editing.